Dynamics of Multi-Agent Systems with Bio-Inspired Active and Passive Sensing

Masoud Jahromi Shirazi

Dissertation submitted to the Faculty of the

Virginia Polytechnic Institute and State University

in partial fulfillment of the requirements for the degree of

Doctor of Philosophy

in

Engineering Mechanics

Nicole T. Abaid, Chair

Mark S. Cramer

Alexander Leonessa

Shane D. Ross

Pablo A. Tarazaga

September 14, 2020

Blacksburg, Virginia

Keywords: Agent-based modeling, Bio-inspired sensing, Flocking, Simultaneous localization and mapping, Sonar

Dynamics of Multi-Agent Systems with Bio-Inspired Active and Passive Sensing

Masoud Jahromi Shirazi

(ABSTRACT)

Active sensors, such as radar, lidar and sonar, emit a signal into the environment and gather information from its reflection. In contrast, passive sensors such as cameras and microphones rely on the signals emitted from the environment. In the current application of active sensors in multi-agent autonomous systems, agents only rely on their own active sensing and filter out any information available passively. However, fusing passive and active sensing information may improve the accuracy of the agents. Also, there is evidence that bats who use biosonar eavesdrop on a conspecific's echolocation sound, which shows a successful example of implementing active and passive sonar sensor fusion in nature. We studied the effect of such information fusion in the framework of two problems: the collective behavior in a multi-agent system using the Vicsek model and the canonical robotics problem of Simultaneous Localization And Mapping (SLAM). Collective behavior refers to emergence of a complex behavior in a group of individuals through local interaction. The Vicsek model is a well-established flocking model based on alignment of individuals with their neighbors in the presence of noise. We studied the aligned motion in a group in which the agents employ both active and passive sensing. Our study shows that the group behavior is less sensitive to measurement accuracy compared to modeling precision. Therefore, using measurement values of the noisier passive sonar can be beneficial. In addition, the group alignment is improved when the passive measurements are not dramatically noisier than active measurements. In the SLAM problem, a robot scans an unknown environment building a map and simultaneously localizing itself within that map. We studied a landmark-based SLAM problem in which the robot uses active and passive sensing strategies. The information provided passively can improve the accuracy of the active sensing measurements and compensate for its blind spot. We developed an estimation algorithm using Extended Kalman Filter and employed Monte Carlo simulation to find a parameter region in which fusing passive and active sonar information improves the performance of the robot. Our analysis shows this region is aligned within the common range of active sonar parameters.

Dynamics of Multi-Agent Systems with Bio-Inspired Active and Passive Sensing

Masoud Jahromi Shirazi

(GENERAL AUDIENCE ABSTRACT)

Group behavior is a fascinating phenomenon in animal groups such as bird flocks, fish schools, bee colonies and fireflies. For instance, many species of fireflies synchronize their flashing when they bio-luminesce. This synchronization pattern is a group behavior created as a result of local interaction formed by sensing individuals in the group. The research question for this dissertation is inspired by comes from group behavior in bats. Bats use echolocation to perceive the environment. They make a sound and listen to the echo of the sound coming back from objects and by analyzing the echo, they can get information about their surroundings. It has been observed that bats may also use the echo of other bats' sound to perceive their environment. In other words they use two different sensors, one is called active sonar since they actively make the sound and listen to its echoes, and the other one is called passive sonar since they just passively listen to the sound generated by other bats. If this information is useful, can we exploit that in design of engineered systems? We investigated these questions using numerical simulation to solve two test bed problems. The first problem is based on a mathematical flocking model in which the individuals in the group align through local interaction. We found out that eavesdropping improves the alignment of the group within a range of parameters in the model which are relevant to the sensing capabilities of the sonar sensors. The other problem is a canonical robotics problem known as the simultaneous localization and mapping (SLAM). In this problem, a robot searches an unknown environment and creates a map of the environment (mapping) and reports the path it takes within the map (localization). We found out that when the robot uses both passive and active sonar, depending on the accuracy of the two sensing approaches, it can improve the accuracy of both the generated map and the robot's path.

To my dear mother, father, and brother

تقدیم به مادر، پدر، و برادر عزیزم

Acknowledgments

First of all, I want to thank my wonderful advisor, Dr. Nicole Abaid, who has always been supportive of me along this journey. Thanks Dr. Abaid!, and no it is not just for your insight, guidance, and every skills you taught me as my advisor. You are more than just an advisor to me. You are like my family here, when mine are living on the other side of the planet. You taught me the most important lesson no book or university could offer, how to be a caring leader. I am blessed to have the opportunity to work with you. I will miss you and all the good times I had here, from our serious discussions in individual and lab meetings to fun birthday parties, lab barbecues and gatherings, and the Thanksgiving dinners you invited me since I was usually the only one still around during Thanksgiving break. I will miss them all for sure but I will never forget, I will never forget your patience in teaching, your humble personality, and the care and respect you showed me and everyone else. I wish I can be your good student and can follow your path in my life and career. Thanks, as well, to my committee members, Dr. Mark Cramer, Dr. Alexander Leonessa, Dr. Shane Ross, and Dr Pablo Tarazaga. I want to thank you Dr. Cramer for being an example of an excellent teacher, the one who knows everything so well that can explain them in such a simple way everyone can understand. I also appreciate you sharing your experience with students as well. I do not forget how you normalized the stress I had before my preliminary exam by telling me the story about that coffee stirring problem or all the late hour meetings we had at

your office talking about continuum mechanics before my preliminary exam. I am thankful to you Dr. Leonessa not just for what I have learned in adaptive control course but also for all the time you somehow opened up for me despite having a very busy schedule. I want to thank you Dr. Ross not just for how you were supportive to me but also for all you have done for the Engineering Mechanics program as the graduate program chair. As a member of GEMS, I had the opportunity to learn by watching how you lead departmental events, present the graduate program and build a cohesive team of faculties, staff and students. I want to thank you Dr Tarazaga, for the fun vibration class you offered, for the emphasis you put on experimental work, and of course for all the informal and constructive conversations we had in your informal office, you know where I am talking about, the coffee shop. I learned a lot from you not only on vibration and acoustics, but also about graduate student life, academic environment and networking. In addition, I want to thank Dr. Sunny Jung who was in my committee before leaving Virginia Tech. I always admire your hard work and passion for science Dr. Jung, and of course I do not recall your face without that friendly smile.

I would like to thank the other faculty members who helped me during my PhD studies. I would like to thank Dr. Jeff Borggaard who accepted me as his student to complete a simultaneous masters degree in Mathematics. Dr. Borggaard, I enjoyed every meeting we had in your office talking about my research. I know it may sound unbelievable, but your knowledge along with your humble and friendly personality made mathematics sound really easy. I like to thanks Dr. William Ford who engaged me more into the fascinating world of bats. I enjoyed doing the clutter project with your team Dr. Ford and I will never forget the memorable night we spent in Shenandoah national park as you were searching for endangered species of bats. Thanks for all you have done for me. I would like to thank Dr. Uwe Tauber for all his time helping me look at my research from a different angle. I also want to thank Dr. Mark Psiaki for teaching me the estimation theory. I admire your dedication in

teaching, holding an extra class session each week to make sure we learn everything we need and thank you for all the fun discussions we had during your office hours.

I like to thank all my previous and current lovely lab mates in the Complex Systems Lab, Subhradeep Roy, Amanda Hashimoto, Aidan Bradley, Eighdi Aung, Nick Orange, Kayla Howes, Irena Shaffer, and Eric Anderson. I have so much fun memories working with all of you that makes it impossible to pick from. I am glad to have you in my life and we will be in touch.

I must also thank the National Science Foundation (NSF) under award 1751498, the United States Geological Survey (USGS) and the Department of Biomedical Engineering and Mechanics at Virginia Tech for financially supporting this study. I am also thankful to all the departmental staff, especially Jessica Grimes for making everything run smoothly.

Last but definitely not least, I cannot be thankful enough to my family, my mother, my father and my brother, for their love, encouragement, advice, belief and support. I could not visit them for all these years and all I got from them was hope and faith. I am thankful to my mother for all she has done for me, to my father for giving me hope and strength, and to my brother that I always looking up to him in my life.

Contents

List of Figures

Chapter 1

Introduction

1.1 Motivation and background information

Collective behavior refers to the emergence of complex patterns through the interactions among a group of agents with a simpler individual behavior. Design of multi-agent systems to perform tasks through collective behavior has been developed as an approach to tackle complicated engineering problems. Compared to a single agent performing the same task, multi-agent systems enjoy more agent simplicity and robustness to failure of some of the agents, at the expense of increasing complexity in their interactions. Therefore, interaction among the agents is a fundamental aspect of study and design of multi-agent systems.

In nature, animal groups are successful at performing different tasks by exploiting collective behavior [1]. Bird flocks, ant colonies, bee swarms and fish schools are examples of social animals whose behavior inspires the design of different algorithms for the dynamics for multi-agent systems. Among animal groups, bats are interesting due to their method of sensing the environment. Many bat species use echolocation, which refers to perceiving the environment

by making a sound and listening to its echo [2]. Echolocation is an example of active sensing, in which the sensor spends energy to actively create a signal and extract information from its reflection, in contrast to passive sensing, in which the sensor only extracts information from the signals received from the environment [3]. Sonar, radar, and lidar are examples of active sensing, while cameras, microphones and thermometers are examples of passive sensors.

The vast majority of multi-agent systems in the literature use passive sensing and a dedicated communication channel. For example, robots in a team may use cameras and image processing to extract information about their environment, and share this information with other agents over a wireless network system. Using active sensing in multi-agent systems, however, comes with challenges and potential benefits. It makes the system prone to signal jamming, which refers to the inability of an agent to distinguish the reflection of its own signal from the others. On the other hand, it can potentially be used as a communication tool among agents.

As an example of a successful multi-agent system with active sensing, bats can be studied to elucidate how to overcome these challenges and exploit the potentials of active sensing. Unlike commonly implemented multi-agent systems with passive sensing, bats do not use a separate communication device to transmit information to peers. In other words, in addition to social calls, they may also use their sensing channel to transfer information. To mention another example, it is known that bats use different calls with different beam patterns to get a balance between range, breadth, and resolution of sensing [4]. Therefore they have the ability to control their sensing range and sensing angle. Also, it has been observed that bats can fly without echolocating for a significant amount of time presumably to prevent signal jamming [5].

These observations on bats' behavior raise research questions on how bats can operate as a multi-agent system. For example, if bats can fly in silence to prevent signal jamming,

how can they maneuver and avoid obstacles during their silent flight? One possible answer to this question is that they interact with the environment through eavesdropping on the sound made by other bats. In other words, bats are able to combine passive listening, i.e. sound source localization, with active echolocation. But how much extra information can agents get by using passive sensing on top of their active sensing? Is it possible to exploit active sensing as a mean of communication among agents who passively eavesdrop on each other? This can reduce the costs and energy of multi-agent systems by eliminating the need to use separate hardware for communication. Also, given the fact that bats can change the angular range of their active sensing, how can changing the sensing geometry and using passive sensing impact the collective behavior of the group?

There are two major approaches to model multi-agent systems. In one approach, the multi-agent system is modeled as a continuous medium and fluid dynamics equations are implemented to predict the system's behavior, such as the study reported in [6]. The other approach is to model the system as a group of individuals interacting through a set of defined behavioral rules. One of the most well-known multi-agent systems is introduced by Vicsek [7], usually referred as the Vicsek model. What makes the Vicsek model interesting is its ability to capture complex group behaviors using simple update rules. The Vicsek model is a flocking model in which each agent assumes the heading direction of its neighbors, subjected to a random noise. The noise is used to model either the inability or unwillingness of the agent to assume the exact calculated heading direction, the *process noise*, or the effect of noisy measurement, the *measurement noise*. Therefore, the group alignment depends on the distribution the noise is sampled from as well as the type of the noise implemented in the model. Each agent depends on its sensing to receive information about other agents in the group. Therefore, the implementation of active sensing, passive sensing, or a combination of both strategies can affect the performance of the group. We study the effect of different

sensing strategies and perform a sensitivity analysis on the parameters used in the model using numerical simulation.

Besides the abstract agent-based modeling, we also study the more practical problem in the setup of a group of robots. We focus on the canonical problem of the Simultaneous Localization And Mapping (SLAM). This problem is a combination of two robotic challenges. The first one is the localization problem, in which the robot has access to a map of the environment and the objective is to localize itself within the map. The second problem is the mapping problem in which the robot have access to its global coordinate, for example through GPS signals, and is tasked to create a map of the features of its unknown environment. In the SLAM problem the robot does not have access to its global position and a map of the environment, and the robot's objective is to build a map using its sensor signals and simultaneously localize itself within that map. The research question we want to answer is whether implementing passive sensing on top of active sensing can be beneficial to solve this problem. An important point to mention here is that we do not study this problem in the context of a multi-agent system since we assume the robots do not share any information with each other. However, if the performance of each robot and the accuracy of its map and localization is improved, sharing information between the robots will improve their performance as well, as shown for two robots in [8]. Therefore, to see the effect of using passive sensing on top of active sensing, we only focus on the performance of a single robot in solving SLAM problem using active and passive sensing.

1.2 Intellectual merit

The intellectual merit of this dissertation includes an abstract agent-based model that combines active and passive sensing to study collective behavior using numerical simulation. In

addition, an algorithm is created to fuse the information gathered by passive sonar with the active sonar information in the framework of the simultaneous localization and mapping problem. Both of these studies demonstrate that the inclusion of passive sensing improves the performance of the system within appropriate ranges of model parameters.

1.3 Dissertation organization

The rest of this dissertation is organized as follows. In chapter 2, we introduce a three-dimensional flocking model to study the effect of process and measurement noise in the group behavior of a multi-agent system. The objective of this study is to find out how sensitive the group behavior of the system is to the error in measurement of each agent. It is important since generally, the passive sensing is generally less accurate than the active sensing. Therefore, the integration of passive sensing can be beneficial if the response of the group is robust to the measurement noise in comparison to the process noise.

After investigating the sensitivity of the flocking model to the measurement noise, in chapter 3, we develop a multi-agent flocking model to study the effect of fusing active and passive sensing in the performance of the model. We perform a numerical sensitivity analysis to find out the range of parameters in which integrating active sensing improves the group behavior of the flocking model.

These abstract agent-based models show that, for some range of parameters, the fusion of passive sensing information can improve the performance of the system. In the next phase, we change our focus to more applied research problems to see if implementing passive sensing can be beneficial. We focus our attention to use active and passive sonar for localization and mapping. First, in chapter 4, we use passive sonar to localize and track a sound source using extended Kalman filter, when a dynamic equation is not known for the sound source

relying on sensor measurements and some a priori information about the source's dynamics. This work is inspired by bats' use of passive sonar without knowing the dynamics of tracked objects using different sensing cues and information.

In chapter 5, we focus on the canonical problem of the landmark based simultaneous localization and mapping when a robot is placed in an unknown environment with unknown number of landmarks and is tasked to build a map of landmark locations and localize itself within the map. We are interested to see how the performance of the robot in solving this problem is affected if the robot uses both active and passive sonar. We implemented extended Kalman filter to solve this problem and used Monte Carlo simulation to perform a sensitivity analysis on the parameters set affecting the robot's performance.

Finally in chapter 6, we summarize the results of this dissertation and conclude that integration of passive and active sensing can improve the performance of the system depending on the sensor parameters. Then we discuss some possible future research directions.

Chapter 2

Comparing the effects of intrinsic and extrinsic noise on the Vicsek model in three dimensions

The content of this chapter have appeared in the proceedings of the 2017 Dynamic Systems and Control Conference: Shirazi MJ, Abaid N. Comparing the effects of intrinsic and extrinsic noise on the Vicsek model in three dimensions. In *Dynamic Systems and Control Conference*, 2017 Oct 11 (Vol. 58288, p. V002T14A010). American Society of Mechanical Engineers.

2.1 Introduction

Collective behavior refers to the emergence of qualitatively complex behavior through interactions among a group of simple individuals. Collective behavior is observed in a variety of living systems such as fish schools [9], bird flocks [10], cells [11], amoeba [12], bacterial

colonies [13], insects [14], mammals [15], and human crowds [16], as well as non-living systems such as nematic liquid crystal [17] and vibrating rods [18]. Despite the vast variety of systems that exhibit collective behavior, its common feature is that the action of individuals is affected by others in the group and leads to different patterns of ordered behavior. Modeling collective behavior and identifying the different emerging patterns can be helpful to understand its possible benefits to engineering systems. A comprehensive review of the state of the art in collective behavior, from experimental and numerical studies to theoretical modeling and control, can be found in [19].

One of the earliest renowned works to simulate collective behavior is a deterministic flocking simulation carried out by Reynolds [20]. Besides simulation, several mathematical models have also been introduced to study collective behavior. There are two major approaches in mathematically modeling collective behavior: considering the system as a continuous media [6], or modeling it as a collection of interacting agents [21]. One of the most famous agent-based models is the so-called Vicsek model described in [7]. This model considers a collection of self-propelled particles in two dimensions, each of them updating its heading to the direction of the average velocity of its neighbors in the presence of noise. As the intensity of noise increases, the collective behavior of the group changes from an aligned, ordered phase to random, unordered phase (referred to as a *phase transition*). Different variations of the Vicsek model are also investigated. As an example, Chaté et. al. review the Vicsek model and expand it by considering polarity for particles and/or their interactions, incorporating the ambient fluid in which particles are moving, and adding cohesion between nearby particles [22]. Also, a generalization of the Vicsek model to three dimensions is reported in [23].

The effect of noise can be introduced in two fundamentally different ways: *intrinsic* (or *process*) noise, and *extrinsic* (or *measurement*) noise. The intrinsic noise, which is used in the original Vicsek model, represents stochastic effects due to the intrinsic nature of the

individual and its free will not to follow exactly the rules of the model. Another way to think about the intrinsic noise is that it compensates for the error between the actual *process* and the expected model rules. The extrinsic noise, however, is used to model the error due to misconception of the environment and other individuals' information. It can be thought of as an error in *measuring* the information, such as location or velocity of other individuals. For example, in flocking of birds, the extrinsic noise can be used to model the error in estimating the velocity vector of the neighboring birds. The intrinsic noise, however, models the incapability of the bird in following the average velocity of the group or its free will to deviate from that. In other words, the intrinsic noise models the decision making process while the extrinsic noise takes the effects of environment into account [24].

The effect of the intrinsic and extrinsic noise on phase transition between ordered and disordered states has been studied in the literature. Phase transitions in the original two dimensional Vicsek model due to intrinsic and extrinsic noise is investigated with numerical simulation in [25]. In addition, the more tractable majority voter model and vectorial network model are used to show that nature of the phase transition (such as the sharpness or continuity) strongly depends on the nature of the noise [25, 26].In these works, phase transition due to intrinsic noise is continuous, while it appears to be discontinuous in the sole presence of extrinsic noise. Also, order in the system seems to be more robust to extrinsic, rather than intrinsic noise [25].

The effect of these two different types of noise on the system depends on the model in hand. In another study about the effect of intrinsic and extrinsic noise published in [27] (in which they call them acting and sensing noise, respectively), the noise is Gaussian and is applied to the adaptive Attractive/Repulsive swarming model from [28]. The authors found out that, unlike the results reported for the original Vicsek model in [25], the system is more robust to acting (intrinsic) noise than sensing (extrinsic) noise.

In this work, we study the three-dimensional Vicsek model with both intrinsic and extrinsic noise using simulations. We seek to understand how the individual noises, and their combination, differential impact the quality of transitions between order and disorder in the system. Furthermore, we explore the relationship between these phase transitions and the density of agents in the domain.

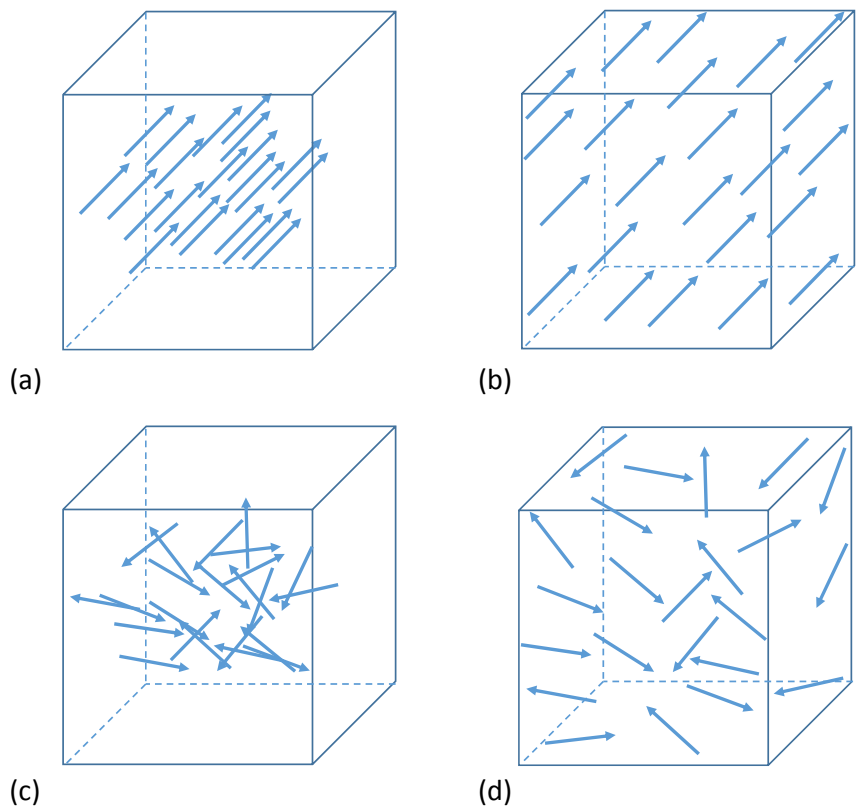

Figure 2.1: Schematic of four different qualitative states of the collective behavior (a) high polarization and low nearest neighbor cohesion, (b) high polarization and high nearest neighbor cohesion, (c) low polarization and low nearest neighbor cohesion, (d) low polarization and high nearest neighbor cohesion

2.2 Modeling

2.2.1 System Dynamics

The three dimensional Vicsek model consists of N self-propelled particles moving at constant speed v_0 in a three-dimensional cube of length L with periodic boundary conditions. For the discrete-time update, each particle assumes the average direction of motion of itself and all the neighbor particles within a sphere of radius R around it. This direction update, however, is disturbed by two random noises: 1) extrinsic (measurement) noise, due to error in estimating the direction of motion of the neighbors, and 2) intrinsic (process) noise due to particle's error in following the desired direction or its free will to deviate from the average direction of motion of the neighbors.

Consider particle i at time step k. The position and heading vectors of this particle are denoted by $\mathbf{x}_i(k) \in \mathbb{R}^3$ and $\mathbf{v}_i(k) \in \mathbb{R}^3$, respectively. The heading vector of this particle at time step $k+1$ is

$$\mathbf{v}_i(k+1) = \mathbf{N}\left(\mathbf{N}\left(\sum_{j\in\Lambda_i(k)} (\mathbf{v}_j(k) + \mathbf{w}_j(k))\right) + \xi_i(k)\right), \tag{2.1}$$

where $\mathbf{N}(\mathbf{u}) = \mathbf{u}/\|\mathbf{u}\|$ gives the unit vector in the direction of $\mathbf{u}$, and $\Lambda_i(k)$ is the index set of all particles in $B_R(\mathbf{x}_i(k))$, the ball of radius R around $\mathbf{x}_i(k)$. Note that $\Lambda_i(k)$ includes the particle i for all time steps. Moreover, $\mathbf{v}_j(k)$ denotes the heading vector of the jth neighbor of particle i at time step k. The vector $\mathbf{w}_j(k)$ models the extrinsic (measurement) noise due to error in estimating the heading direction of neighbor j. The vector $\xi_i(k)$ is used to deviate the final heading direction from the average of heading directions of neighbors to model the intrinsic (process) noise. At each time step and for each i or j, the measurement noise and process noise vectors are assumed to be independent realizations of three dimensional

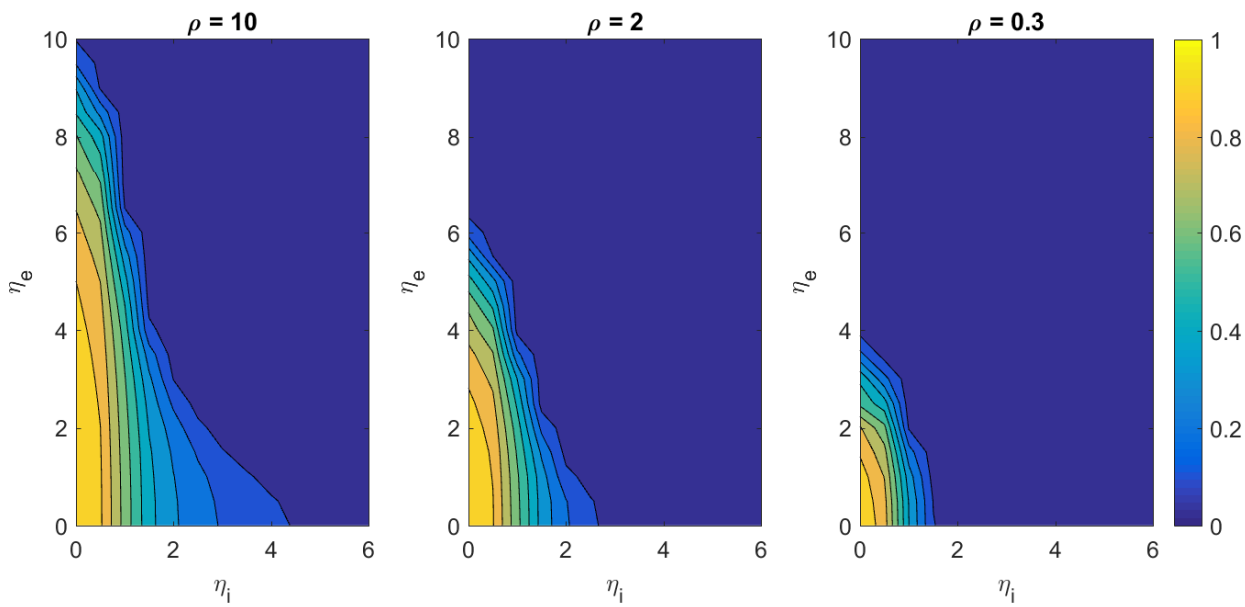

Figure 2.2: Polarization vs amplitude of extrinsic noise and intrinsic noise with $N = 1000$, $R = 1$, and $v_0 = 0.03$.

random vectors uniformly distributed over spheres of radius η_e and η_i, respectively. Note that all heading vectors have length 1 by design.

Using this self-propelled particle model, the updated position of the particle i is

$$\mathbf{x}_i(k+1) = \mathbf{x}_i(k) + v_0\mathbf{v}_i(k+1), \tag{2.2}$$

where v_0 is the constant speed of all particles.

If particles measure exactly the direction of motion of each neighbor j, the extrinsic noise vector $\mathbf{w}_j(k)$ vanishes and Eqn. (3.1) reduces to the three dimensional Vicsek model described in [23]. Also, if the uncertainty is only due to measurement error, the intrinsic noise vector $\xi_i(k)$ vanishes and Eqn. (3.1) becomes the three dimensional version of the extrinsic noise discussed in [25].

2.2.2 Order Parameters

The polarization of the group is used as order parameter, which can be calculated as

$$P(k) = \frac{1}{N} \left\| \sum_{i=1}^{N} \mathbf{v}_i\,(k) \right\|, \tag{2.3}$$

This parameter is the magnitude of the average of the linear momentum of the system. The polarization is a number between zero and one and the higher its value is, the more aligned is the group. We consider this alignment to be emergent order in the model.

To investigate the cohesion of the group, we compute the distance to the nearest neighbor averaged over all particles [29], that is

$$C(k) = \frac{1}{N} \sum_{i=1}^{N} \min_{\substack{j=1,\ldots,N,\\ j\neq i}} \|\mathbf{x}_i\,(k) - \mathbf{x}_j\,(k)\,\|, \tag{2.4}$$

This parameter is always positive, with lower values indicating that all particles are nearby at least one neighbor and higher values indicating more isolated particles.

Based on values of polarization and nearest neighbor cohesion, it is possible to define four different qualitative states for collective behavior as illustrated in Fig. 4.1. When the polarity is high and the nearest neighbor cohesion is low, all the particles move together in an ordered way in one or some clusters (Fig. 4.1(a)). When polarization and nearest neighbor cohesion are both high, the group moves in an ordered way but the particles are more spread away(Fig. 4.1(b)). In low polarization and low nearest neighbor cohesion values, the group forms one or several clusters yet the particle movements is disordered (Fig. 4.1(c)). Finally, low polarization and high nearest neighbor cohesion value corresponds to the situation when the particles are far away and showing disordered movement (Fig. 4.1(d)).

Table 2.1: The number of steps used to simulate the results for different densities and the maximum standard deviation of polarization σ_p and nearest neighbor cohesion σ_c.

Density	Number of Steps	$\max(\sigma_p)$	$\max(\sigma_c)$
10	533	0.0511	0.0019
2	533	0.0673	0.0042
0.3	1332	0.0862	0.0070

2.3 Simulation Results

Numerical simulation is used to study the combined effect of intrinsic and extrinsic noise on this model for systems with $N = 1000$, $R = 1$, and $v_0 = 0.03$. The initial condition for particles' position and heading vectors are chosen randomly in the cube of side length L and the unit sphere, respectively, with uniform distributions. The intrinsic and extrinsic noises are considered to be random vectors uniformly distributed over a sphere with raduis η_i and η_j, respectively. We vary three control parameters: the average density of the particles, $\rho = N/L^3$, the amplitude of the extrinsic noise, η_e, and the amplitude of intrinsic noise, η_i.

For each simulation, we iterate the model until we achieve a stationary distribution for polarization, which occurs at a different number of time steps depending on model parameters as reported in Tab. 2.1. The number of time steps reported is the total simulation length after an initial transient of 50% of this length. We report the mean polarization and mean nearest neighbor cohesion from these stationary distributions in the following results.

Polarization versus process and measurement noise amplitude are shown in Fig. 2.2 for three different values of density. We can see that polarization decreases monotonically with increasing noise amplitude whether it be intrinsic or extrinsic noise. We call the decreasing of the polarization from higher values to near zero with increasing noise a phase transition. By comparing horizontal versus vertical slices of each contour plot, the phase transition occurs

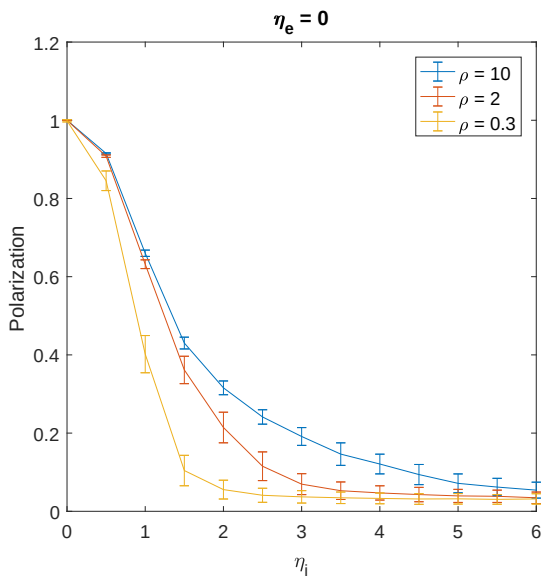

Figure 2.3: Polarization vs amplitude of intrinsic noise with $\eta_e = 0$, $N = 1000$, $R = 1$, and $v_0 = 0.03$.

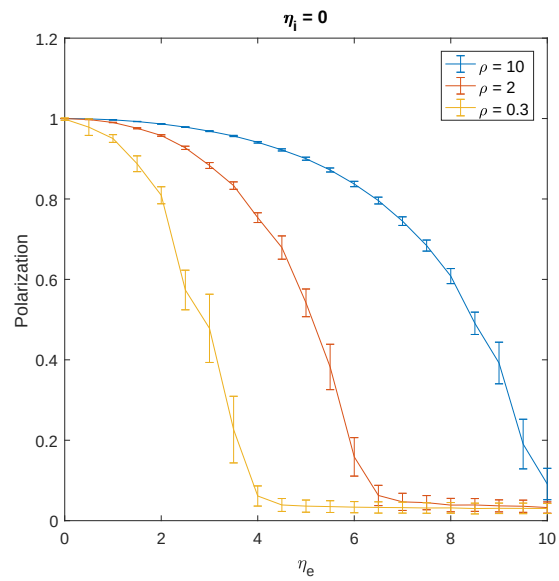

Figure 2.4: Polarization vs amplitude of extrinsic noise with $\eta_i = 0$, $N = 1000$, $R = 1$, and $v_0 = 0.03$.

for lower values of η_i than for η_e. That is, the curve varying η_e when $\eta_i = \eta^*$ lies at or above the curve varying η_i when $\eta_e = \eta^*$. As the density of particles is decreased, the region of higher polarization (which occurs when η_e and η_i are low) shrinks in size but maintains the relative relationship between the two noises.

The special case in which the extrinsic noise is zero is depicted in Fig. 2.3 for three values of particle density. In this case, the only noise in the system is the intrinsic noise. We see that increasing the noise amplitude destroys order in the system, but the phase transition occurs at higher values of η_i when the particle density increases. The other marginal case where the extrinsic noise is the only uncertainty in the model is depicted in Fig. 2.4. This plot shows similar trends as for the system with only intrinsic noise in Fig. 2.3, but the phase transition for fixed particle density happens at higher values of noise amplitude when the noise is only extrinsic.

The nearest neighbor cohesion of the group calculated by Eqn. (3.4) is plotted as a function

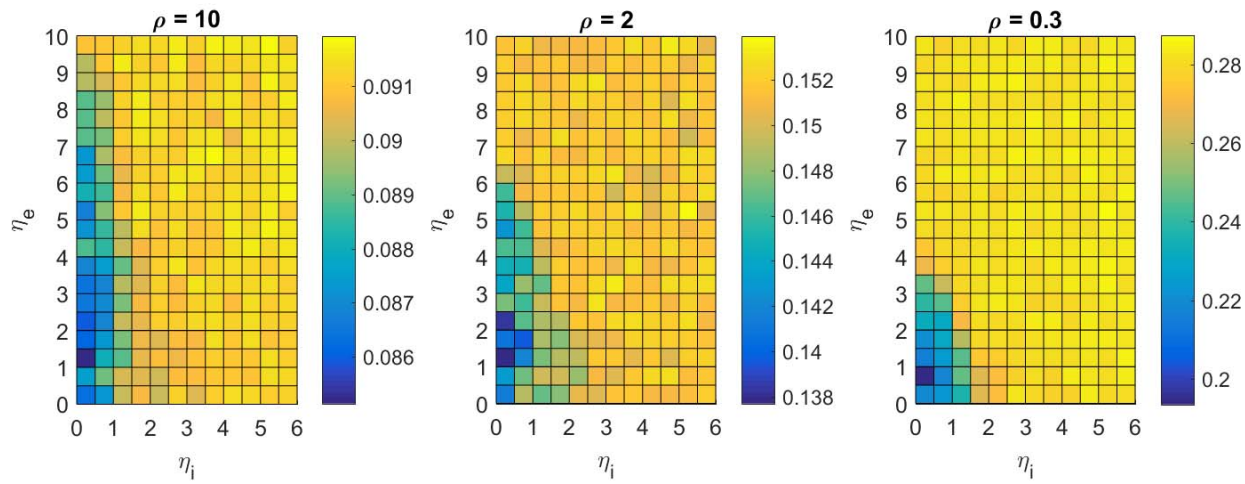

Figure 2.5: Cohesion vs amplitude of extrinsic noise and intrinsic noise with $N = 1000$, $R = 1$, and $v_0 = 0.03$.

of intrinsic and extrinsic noise in Fig. 2.5. The results show that it is harder to maintain cohesion when the density is low or either intrinsic or extrinsic noise is strong.

2.4 Discussion

As it is shown in Fig. 2.2, the polarization is one when there is no noise in the system, but as the amplitude of either intrinsic or extrinsic noise increases, the polarization drops. Also, the polarization is more robust to increasing extrinsic noise compared to intrinsic noise. This phenomenon can be explained by noting that the extrinsic noise in Eqn. (3.1) appears inside a summation and the final result is normalized. Therefore, loosely speaking, the effect of extrinsic noise is *averaged out* in the final heading direction. Since the random noise vectors are uniformly distributed in terms of direction, their sum has zero mean, which increases the robustness of the model to extrinsic noise. It follows that, the higher the density of the group, the more averaging is performed on realizations of the extrinsic noise, and thus the polarization is less affected by this noise, as demonstrated in Fig. 2.2. Nevertheless, intrinsic

noise is added to the model update after summing the effects of interactions with neighbors, and it directly impacts polarization.

The change in polarization versus intrinsic noise when extrinsic noise is zero is shown in Fig. 2.3. As mentioned in the model, this situation would recover the three dimensional Vicsek model, which can be verified by the close correspondence between Fig. 2.3 and Fig. 2 in [23]. Similarly, the change in polarization versus extrinsic noise when intrinsic noise is zero is illustrated in Fig. 2.4. In this case, the polarization is more robust to measurement noise, which corroborates the results in two dimensions given in [25].

It is worth noting that the shape of the curves showing a phase transition for our three dimensional model with only extrinsic noise (Fig. 2.4) are strikingly different from those reported in Fig. 1 in [25] for a two dimensional model with extrinsic noise, which are described therein as "discontinuous". More investigation is needed to properly explain this observation, which may evidence either qualitatively different dynamics or numerical artifacts from the implementation of simulations. Barring numerical artifacts, one possible hypothesis is that the extra *freedom of movement* particles have in three dimensional space offers particles more paths with higher alignment for intermediate values of noise.

Moreover, noticing the shape of level curves in Fig. 2.2, we see that increasing extrinsic noise makes the phase transition happen at lower amplitudes of intrinsic noise. This shows that the intrinsic and extrinsic noises have combine effects to reduce order in the system. Therefore, in application problems where extrinsic noise is inevitable, these results predict that the phase transition would happen at lower intrinsic noise amplitudes than given by the Vicsek model.

The effect of density in the presence of intrinsic or extrinsic noise is evidenced in characteristics of the phase transition. By comparison of the Fig. 2.3 and Fig. 2.4, it can be seen that,

while increasing density makes the phase transition more smooth in sole presence of intrinsic noise, it translates the phase transition to a higher value of noise when extrinsic noise is the only uncertainty of the system. In both cases, increasing density makes the system capable of maintaining higher polarization for a fixed value of the noise parameter. However, systems with extrinsic noise retain the sharpness of the phase transition and systems with intrinsic noise do not.

By comparing results for nearest neighbor cohesion in Fig. 2.5 and polarization, we can see that agents in the system stay closer to each other when the density is high and the noise value is low. In fact, the system is more cohesive when its particles are more aligned, since low values of cohesion indicate that particles are closer to each other on average. This cohesion emerges even though an attraction rule is not imposed directly by the model, which supports such emergent spatial properties known to be present in the two-dimensional Vicsek model [22]. Therefore, these results suggest that in three dimensional Vicsek model, only two of the four possible states exists in steady state condition, which supports that polarization induced cohesion unlike other models with attraction repulsion zones like the model presented in [21].

2.5 Conclusion And Future Work

In this paper, the combined effect of extrinsic and intrinsic noise on the three dimensional Vicsek model is investigated using numerical simulation. It has been shown that, similar to the two dimensional model, the polarization of the group is less robust to intrinsic noise than extrinsic noise. Also the phase transition happens at smaller values of the intrinsic noise when the extrinsic noise value increases, which is supported by results on this model in two dimensions. However, the phase transition due to extrinsic noise in the three dimensional case is less sharp than in the two dimensional case. Also, the particles stay close to each

other and more aligned particles make the group more cohesive.

Future work on this problem will be to validate simulation results with other analytical models, such as the majority vote model or vectorial network model. In addition, we can rigorously characterize the nature of phase transition (e.g its order) in the three dimensional Vicsek model in present of intrinsic and extrinsic noise studied here. Finally, the effect of other model parameters, such as number of agents, sensing radius and agent velocity, on the collective behavior of the system with intrinsic and extrinsic noise will also provide a more holistic view of these dynamics in the future.

Chapter 3

Collective behavior in groups of self-propelled particles with active and passive sensing inspired by animal echolocation

The content of this chapter have appeared in Physical Review E: Shirazi MJ, Abaid N. Collective behavior in groups of self-propelled particles with active and passive sensing inspired by animal echolocation. *Physical Review E*, 2018 Oct 8;98(4):042404.

3.1 Introduction

When a group of individuals interacts among themselves using simple rules, they can exhibit complex behavior as a whole. This phenomenon is referred to as *collective behavior* and

has manifested in many physical systems such as vibrating rods [18], nematic liquid crystal [17], and active colloids [30]. It is also observed in living systems such as fish schools [9], bird flocks [10], primates [15], insects [14], cells [11], amoeba [12], bacterial colonies [13], and human crowds [16]. Depending on the rules of motion and interaction between individuals, the group can show different patterns of ordered behavior such as aligned movement or milling.

Modeling collective behavior is a problem that has been approached by researchers from different communities. The agent-based model provided by Vicsek [7], which is commonly referred as the Vicsek model, is one of the most well-studied due to its ability to capture complex group behaviors with a simple update rule. In this model, each agent or particle is moving with constant speed in a two-dimensional square with periodic boundary conditions and, at each time step, the particles take the average direction of their neighboring particles, subjected to noise. The polarization, which is the averaged linear momentum of the group, is considered as an order parameter for aligned movement. As the intensity of the noise increases to some critical value, the order parameter drops dramatically which shows a *phase transition* in the group. A three-dimensional version of the Vicsek model has been more recently published in [23]. The paper published by Chaté et al. expands the Vicsek model by adding polarity to particles and their interaction, as well as including the effect of an ambient fluid and cohesion between nearby particles in both two and three dimensions [22]. Besides the Vicsek model which is based on sensing neighbors' direction of motion, we note that collective behavior may be seen in models that use alternative sensing strategies, see for example the position-based model in [31]. A thorough review of collective motion, its manifestation in different research areas, and different suggested models can be found in [19].

The behavior of particles in the Vicsek model is highly dependent on their ability to sense

their environment. Inspired by sensory limitations in biological and robotic systems, recent models have sought to explore the role of a so-called *sensing angle*. This angle defines the portion of the circular/spherical neighborhood around an agent that it can perceive, and thus the information it can use for the alignment protocol. In addition to the phase transition that can be found by changing noise on alignment, the relationship between sensing angle and polarization is still an active area of research. Nguyen et al. demonstrate a phase transition with changing sensing angle in the two-dimensional Vicsek model [32], with the critical noise value defined where polarization variance is maximized over different sensing angles. They report that the critical noise increases with increasing sensing angle. Also, they show by simulation that the critical noise converges to some value as the number of agents increases and this value is negligible for angles less than $\frac{\pi}{2}$. Therefore, no phase transition with respect to noise happens for the case with sensing angle is less than $\frac{\pi}{2}$. Durve and Sayeed use the same model to study polarization as sensing angle is varied [33]. The authors find that the phase transition is of the first order when sensing angle is varied, while it is of the second order when the radius of the circular neighborhood around the particle is varied. In [34], the two-dimensional deterministic Vicsek-like model with angle restriction is considered and an optimal angle is found which leads to the fastest alignment of particles. The three-dimensional version of this problem is also considered in [35], however the final results are hard to interpret since the equations may be written in two rather than three dimensions. Decoupling the directions of sensing and motion may also lead to significant decreases in the time to align, as is shown in [36].

Vicsek-like agent-based models are often used to capture collective behavior in animal groups and their engineered analogs, robotic swarms. To interact with and gather information from the environment, individuals rely on sensing mechanisms. These mechanisms can use different signals such as light [10], sound [2], chemicals [37], and electrical charge [38]. Sensors can

be categorized in two different groups, *active sensors* and *passive sensors*. Active sensors use energy to create a signal and gather information about the environment from its reflection. Radar, sonar, and lidar are examples of active sensors. In contrast, passive sensors analyze signals already present in the environment [3]. Cameras, microphones, and thermometers are examples of passive sensors. Since many animal groups rely on passive sensing, such as vision, most models for biological systems are designed with only passive sensing. In contrast, groups that use active sensing may have different communication modalities since their sensing signals are broadcast and thus interceptable by design.

Bat swarms are an example of highly successful animal groups that use active sensing, that is, echolocation for navigation [2]. Collective behavior using active sensing comes with unique features, as are reported in bats. As an example, it is known that bats use different calls with different beam patterns to get a balance between range, breadth, and resolution of sensing [4]. Therefore they have the ability to control their sensing range and sensing angle. Another example of a feature unique to active sensing is the interference of the reflected signals made by different bats in the group, sometimes referred to as *jamming*. Bats use different strategies such as changing sound frequency [39], temporal characteristics of the sound [40], direction of the sound [41] or even flying without echolocating [5]. A summary of the research done on bats and whale echolocation can be found in [4].

The silent flight of bats observed in [5], which the authors suggest may prevent jamming, raises the question of how bats can maneuver and avoid obstacles during their silent flight. One possible answer to this question is that they interact with the environment through eavesdropping on the sound made by other bats. In other words, bats are able to combine passive listening, i.e. sound source localization, with active echolocation. Given the fact that bats can also change the sensing angle of their active sensing, we may ask how can changing the sensing angle and using passive sensing impact the collective behavior of the group.

Inspired by bats' sensing, this study seeks to investigate whether augmenting an active sensing mechanism with passive sensing can improve the collective behavior of the group. We study the collective behavior of a group of particles using both active and passive sensing in the presence of noise through a three-dimensional agent-based model in the spirit of Vicsek. Using polarization as an order parameter, we study phase transitions evidencing collective behavior as noise magnitude and sensing angle change.

3.2 Self-propelled particle model

The self-propelled particle model consists of N particles moving in a three-dimensional cubic domain of length L with constant speed v_0. The boundary condition of the cube is assumed to be periodic. Each particle has a spherical sensing space with radius R. This sensing space is split up into an active sensing region, i.e. points inside a cone with opening angle 2θ, and a passive sensing region which covers all the points outside the active sensing cone. All the particles within distance R of a specific particle, including the particle itself, are called its *neighbors*. Whether a neighbor is located inside the cone of active sensing or outside of it can be used to divide the neighbors into two disjoint sets which we call *active neighbors* and *passive neighbors*, respectively. The particle itself is considered to be an active neighbor. This geometric partitioning of neighbors is inspired by the angular limitation of active sonar, which occurs in a fairly narrow beam, while passive sonar can be performed omnidirectionally.

Particle i at time step k has position vector $\mathbf{x}_i(k)$ and heading vector $\mathbf{v}_i(k)$, which is a unit vector defining the direction of motion of the particle. At time step $k+1$, this particle

assumes the following heading vector:

$$\mathbf{v}_i(k+1) = \mathbf{N}\left(\frac{n_\mathrm{a}\mathbf{v}_i^\mathrm{a}(k+1) + n_\mathrm{p}\mathbf{v}_i^\mathrm{p}(k+1)}{n_\mathrm{a}+n_\mathrm{p}}\right), \tag{3.1}$$

where n_a and n_p are the number of active and passive neighbors, respectively, and $\mathbf{N}(\mathbf{u}) = \mathbf{u}/\|\mathbf{u}\|$ returns a unit vector in the direction of vector $\mathbf{u}$. Finally, $\mathbf{v}_i^\mathrm{a}(k+1)$ and $\mathbf{v}_i^\mathrm{p}(k+1)$ model the contribution of the active and passive neighbors' headings in the particle's heading direction, which are calculated as follows:

$$\mathbf{v}_i^\mathrm{a}(k+1) = \mathbf{N}\left(\mathbf{N}\left(\sum_{j\in\Lambda_i^\mathrm{a}(k)} \mathbf{v}_j(k)\right) + \xi_\mathrm{a}(k)\right), \tag{3.2}$$

$$\mathbf{v}_i^\mathrm{p}(k+1) = \mathbf{N}\left(\mathbf{N}\left(\sum_{j\in\Lambda_i^\mathrm{p}(k)} \mathbf{v}_j(k)\right) + \xi_\mathrm{p}(k)\right), \tag{3.3}$$

where $\Lambda_i^\mathrm{a}(k)$ and $\Lambda_i^\mathrm{p}(k)$ are index sets of active and passive neighbors, respectively. The noise vectors $\xi_\mathrm{a}(k)$ and $\xi_\mathrm{p}(k)$ are random vectors uniformly distributed over spheres with radii η_a and η_p, respectively.

According to equation (3.1), each particle assumes a weighted average of the heading of its neighboring particles as its new heading direction. In other words, each particle calculates the heading of its neighbors using active and passive sensing separately, disturbed by a noise. The particle then computes the heading direction for the next time step by assigning a weight to each direction based on the number of active and passive neighbors. A schematic of the heading direction update is depicted in figure 4.1.

The average heading vectors of active and passive neighbors are disturbed by noises $\xi_\mathrm{a}(k)$ and $\xi_\mathrm{p}(k)$, respectively. These noise vectors, that we call *active noise* and *passive noise*, are assumed to be uniformly distributed over spheres of radii η_a and η_p, respectively. The

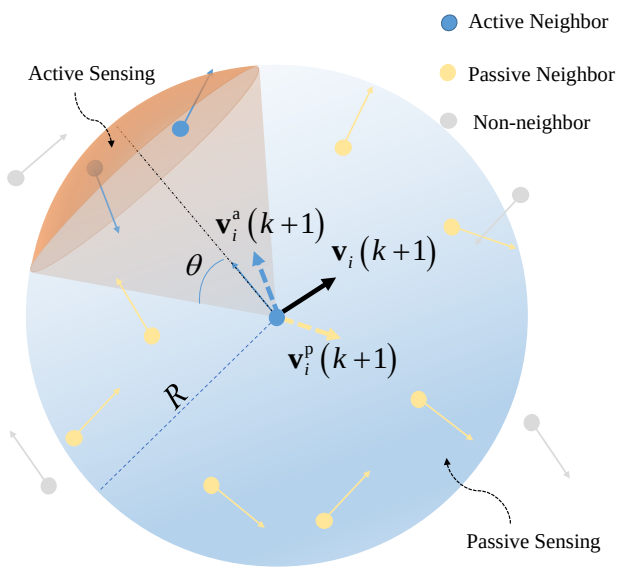

Figure 3.1: A schematic of a particle and its active and passive neighbors. Blue and yellow dashed vectors show the average heading of active and passive neighbors, respectively, and the calculated heading of the particle at next time step is shown as a black vector.

two noises are used to model incapability of the particle to head exactly toward the average heading vector of the active or passive neighbors due to muscle or actuation resolution. This randomness can also be seen as the particle's *free will* to deviate from the average heading of the neighbors based on the particle's *trust* in its neighbors or in the accuracy of its sensing. Since the particle interacts with active and passive neighbors via different sensing approaches, it is rational to consider different values for active noise and passive noise to model different levels of trust in these approaches.

The modeling selection of differentiating between active and passive sensing through the separate, randomly perturbed updates in equations (3.2) and (3.3) seeks to capture behavioral responses inspired by bats' use of echolocation and eavesdropping. These two types of sensing result in information which is known to be more or less accurate by design. The physics of active and passive sensing is incorporated into the choice of geometry for the sensing regions. The relative trust in the accuracy of information from active and passive

sensing is incorporated into the noises ξ_{a} and ξ_{p}. However, the model is not intended to capture the physics and biology governing active or passive sensing, instead focusing on the relationship between individual and collective behavior in groups of particles.

Once the heading vector of particle i in the next time step is calculated, the updated position of this particle can be found as

$$\mathbf{x}_i(k+1) = \mathbf{x}_i(k) + v_0 \mathbf{v}_i(k+1). \tag{3.4}$$

It should be noted here that since each particle is assumed to be its own active neighbor, n_{a} is at least one and therefore, equation (3.1) is well defined. Also, in the special case when $\theta = \pi$, all the neighbors are active and the model is reduced to the three-dimensional version of the Vicsek model with noise strength η_{a}. When $\theta = 0$, however, this model will not recover the Vicsek model since the particle itself is an active neighbor and the noise term in equation (3.2) will be added to that in equation (3.3), and the resulting noise will not be uniformly distributed over a sphere.

To study the collective behavior of the group, we consider the order parameter of *polarization*, which is the magnitude of the averaged group linear momentum. Polarization of a group of particles can be defined as

$$P(k) = \frac{1}{N} \left\| \sum_{i=1}^{N} \mathbf{v}_i\left(k\right) \right\|. \tag{3.5}$$

Polarization is a real number between zero and one, where larger values indicate higher alignment in the group. When the value of polarization is equal to one, it is associated with a perfectly aligned group, while polarization close to zero shows that the particles are performing random walks.

Table 3.1: Simulation parameters

Variable	**Symbol**	**Value**
Cubic domain side length	L	15
Density of particles	ρ	1
Number of particles	N	3375
Particle speed	v_0	0.03
Sensing range (linear)	R	1
Sensing angle	θ	$[0, \pi]$
Passive sensing noise amplitude	η_{p}	$\{0, 0.6, 1.2, 1.8\}$ and None
Active sensing noise amplitude	η_{a}	$\{0, 0.2, \ldots, 1.8\}$
Total simulation time steps	K	300,000
Time steps omitted as transient	-	30,000

3.3 Simulations

After defining the model, numerical simulation is used to investigate the effect of active sensing noise amplitude η_{a}, sensing angle θ, and passive sensing noise amplitude η_{p} on the polarization. The model considers particles moving in three dimensions inside a cube with length $L = 15$. All particles have a sensing range of $R = 1$ and are moving with constant speed $v_0 = 0.03$. The average density, which is equal to the number of particles per unit volume, is set to be equal to one. We vary two control parameters, η_{a} and θ, for different values of η_{p}. Simulations are done for 5 different cases: $\eta_{\mathrm{p}} = \{0, 0.6, 1.2, 1.8\}$ and no passive sensing, which refers to the case when particles use only active sensing, i.e. $v_i(k+1) = v_i^{\mathrm{a}}(k+1)$. The sensing angle θ changes from zero to π, with increment of $\pi/36$, and η_{a} takes values between 0 and 1.8, with increment of 0.2. For each simulation, the model is iterated in time until it reaches to a stationary condition. Rigorously, we consider the polarization to be stationary if it satisfies the first-order weak stationarity condition, in which the first moment of polarization remains constant [42]. After omitting 30,000 time steps to capture the transient, the polarization is averaged over moving windows of length 30,000 time steps

which proceed with an increment of 100 time steps. To test whether the average polarization over the moving windows is constant, we compute the coefficient of variation of these values. This quantity does not exceed 7% for all considered simulation parameters, which we take to satisfy the qualitative definition of stationarity above. Simulation parameters are condensed in table 5.1. For the analysis below, we report the mean polarization averaged over all time steps after the omitted transient for each set of simulation parameters.

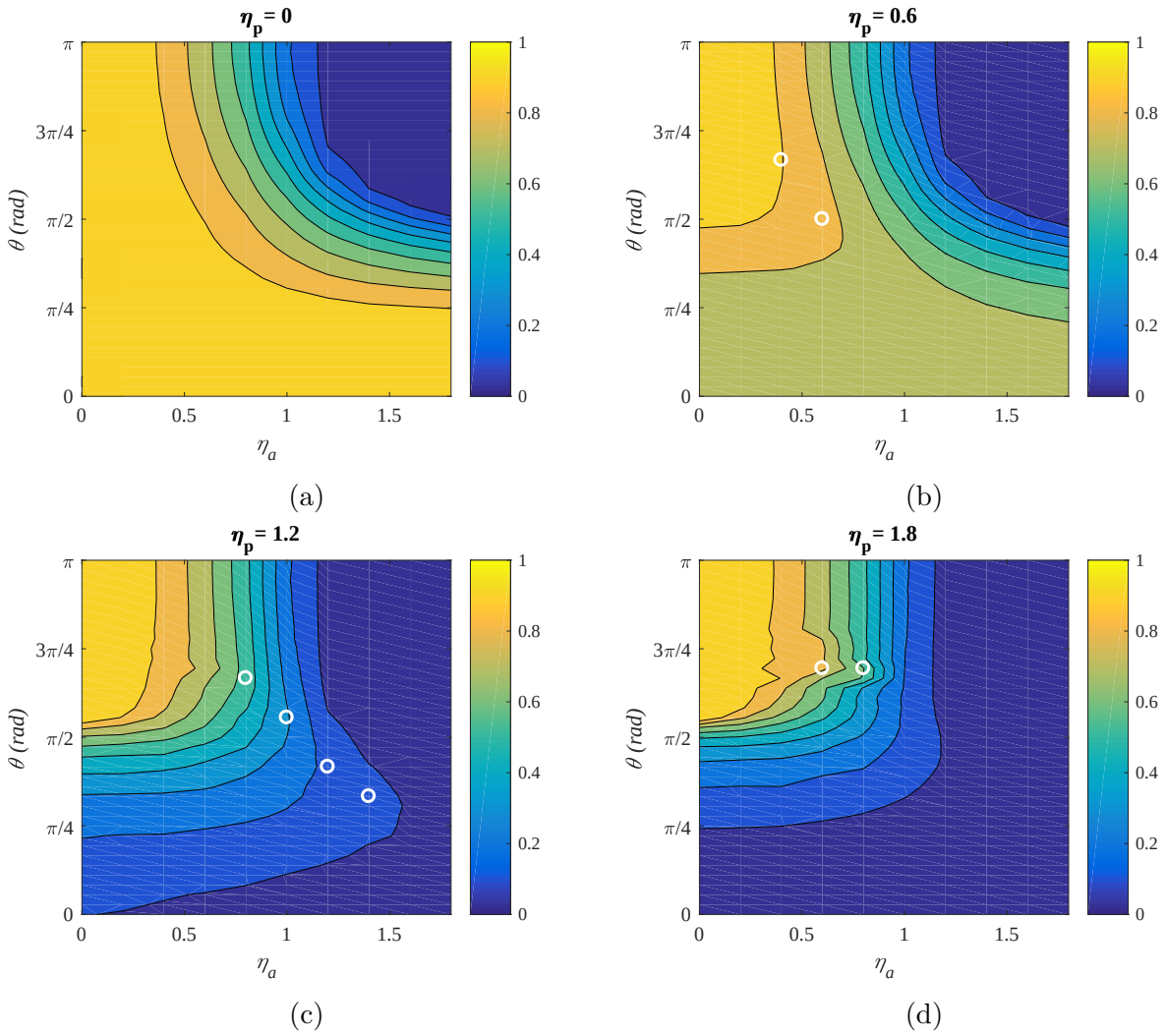

Figure 3.2: Averaged polarization as a function of sensing angle and active noise amplitude for different values of passive noise amplitude. The white circles shows the maximum value of polarization for fixed η_a.

3.4 Results and Discussion

The averaged polarization of the group is shown in figure 3.2 as a function of sensing angle and active noise magnitude for different conditions of passive sensing. In all considered cases of passive sensing, when the sensing angle is π, the trend of the model is consistent with the three-dimensional Vicsek model. Namely, the polarization is high for small values of η_{a}, and decreases to zero with increasing noise. Also, at any fixed sensing angle and passive sensing condition, the polarization decreases monotonically as η_{a} increases. Moreover, when the sensing angle is fixed, at any active noise magnitude, the polarization decreases as the magnitude of passive noise increases. As either noise is increased beyond a critical value, the polarization appears to approach a limit.

The four plots in figure 3.2 show the effects of adding passive sensing with different η_{p} to the active sensing with restricted angle. In contrast to the effect of passive noise, there are some values of η_{a} for which polarization shows a maximum with increasing θ. This occurs when the active noise does not dominate passive noise, that is, when η_{a} is either less than or approximately equal to η_{p}. The white circles show the locations of maxima in polarization for fixed values of η_{a} as θ is varied. For sets of simulations with fixed η_{a} where no averaged polarization was above one standard deviation of all other simulations in the set, we did not report the maximum. These cases generally referred to averaged polarizations that were constant or changed monotonically as θ increased.

Figure 3.3 shows the case with no passive sensing. When the sensing angle is less than a threshold, approximately equal to $\pi/2$, the ordered phase exists only at very small values of η_{a}. This is similar to results reported in [32] in which it is shown that in the two-dimensional Vicsek model with variable sensing angle, for angles smaller than $\pi/2$, the critical noise is very small and the ordered phase does not practically exist. As the sensing angle increases

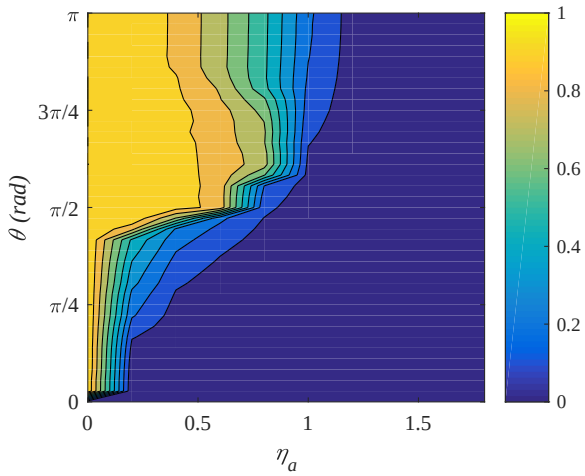

Figure 3.3: Averaged polarization as a function of sensing angle and active noise amplitude when only active sensing is implemented.

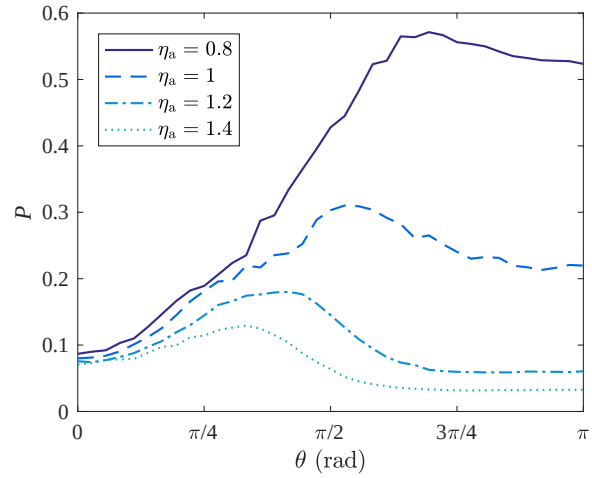

Figure 3.4: Averaged polarization at different active noise amplitude as a function of sensing angle when $\eta_{\mathrm{p}} = 1.2$

above this threshold, the range of active noise magnitude where the ordered phase exists ($P \backsimeq 1$) dramatically increases. In other words, if the magnitude of noise is not too large, there is a sharp phase transition as the sensing angle increases. This sharp phase transition is also reported for two-dimensional model in [33]. Moreover, the phase transition as the sensing angle increases in the presence of passive sensing (figure 3.2) appears more gradual in comparison to the phase transition when particles only use active sensing in figure 3.3. Moreover, the range of active noise in which the ordered phase exists is not monotonically increasing with θ and shows some optimal sensing angle. In other words, the optimal sensing angle is associated with a system whose order is more robust to the introduction of active noise. This is similar to the results reported in [34] for the two-dimensional Vicsek model, except they defined optimality based on how fast polarization reaches to 1 when there is no noise in the model. For small values of active noise magnitude, e.g. $\eta_{\mathrm{a}} < 0.6$, phase transition occurs with respect to increasing θ, while for larger values of active noise magnitude, the phase transition is absent since the ordered phase is never reached.

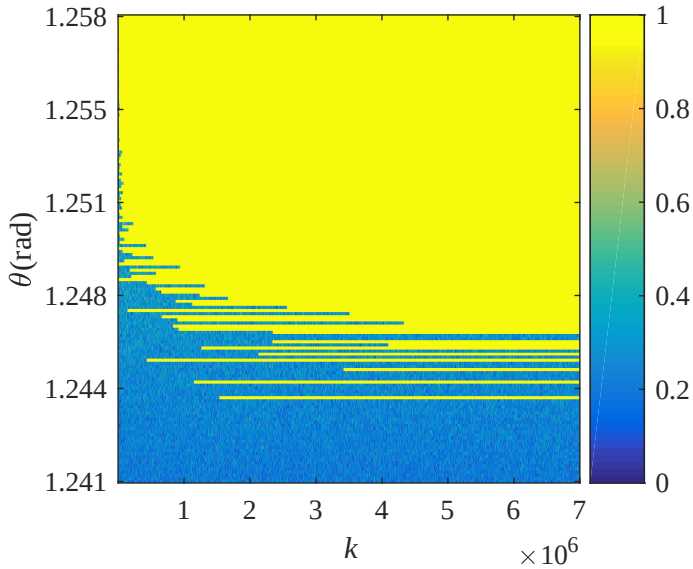

Figure 3.5: Time series of the instantaneous polarization near critical sensing angle at $\eta_{\mathrm{a}} = 0.4$ for 150 different values of sensing angle with resolution 0.0035 radians.

In the presence of passive noise, however, the polarization does not monotonically increase as the sensing angle increases for all value of active noise magnitude. When particles use passive sensing and active sensing together, depending on the relative values of active noise magnitude and passive noise magnitude, the collective behavior can be divided into three different cases: $\eta_{\mathrm{p}} >> \eta_{\mathrm{a}}$, $\eta_{\mathrm{p}} \backsimeq \eta_{\mathrm{a}}$, and $\eta_{\mathrm{p}} << \eta_{\mathrm{a}}$. In the first case, when the sensing angle is large, the behavior of the system is similar to the case with no passive sensing since the number of passive neighbors is negligible comparing to the number of active neighbors. At smaller sensing angles, however, especially when the active noise is not close to zero, exploiting passive sensing improves polarization of the group compared to the no-passive-sensing case. For example, the polarization when $\eta_{\mathrm{a}} = 0.4$ and $\theta = \pi/4$ is 0.7776 when $\eta_{\mathrm{p}} = 0.6$ and 0.0748 when no passive sensing is allowed. This order-of-magnitude improvement to system order is due to extra information that is ignored when using only active sensing. It is notable that this boost occurs even though the extra information from passive sensing is noisy compared to its active counterpart.

For the second case When active noise magnitude and passive noise magnitude are close to each other, according to equations (3.1)-(3.3), the effective noise acting on the system is the sum of two zero-mean noises which are uniformly distributed over the sphere and therefore, their summed effect has a smaller magnitude compared to those of the original summands. As a result, the maximum polarization occurs at more restricted angles compared to the no passive sensing case. This effect of averaging zero-mean noises can be seen by considering the line plots in figure 3.4, which uses $\eta_{\mathrm{p}} = 1.2$ and captures vertical slices of figure 3.2(c) at $\eta_{\mathrm{a}} = 0.8, 1, 1.2$, and 1.4. The maxima of polarization occur at approximately $\theta = 2.182, 1.658, 1.309$ and 1.047 rad respectively. This behavior is expected since, as the particle's trust of its active neighbors decreases, it relies more on passive neighbors to get more information necessary for alignment, which is achieved by reducing the sensing angle.

For the third case when passive noise is much smaller than active noise, the interpretation of the noises as trust of the sensing process means that passive sensing is trusted dominantly over active sensing by the particle. Therefore, the polarization increases as the sensing angle decreases, and more neighbors are passive neighbors than active. The level curves of polarization in this case are interesting. As it can be seen in figure 3.2(a), the larger sensing angle with smaller active noise has the same polarization as smaller sensing angle with larger active noise. It can be interpreted as a trade off between using too many active neighbors with moderate active noise versus a group of less active neighbors with strong noise condition and a group of passive neighbors with small noise. Moreover, it seems that as active noise magnitude increases, the polarization approaches a limit at each sensing angle. This occurs because, when the active noise magnitude is high, the sum of the direction of the active neighbors will be negligible compared to the active noise vector. In other words, the information gathered by active neighbors is so corrupted by noise that it is effectively just random with no useful information.

As an interesting side note, comparison between polarization in the no passive sensing case of figure 3.3 and all the cases fusing active and passive sensing in figures 3.2a-3.2d suggests that, in presence of passive sensing, the phase transition is happening more gradually as the sensing angle changes compared to the no passive sensing case. One explanation for this difference could be that the extra information gathered with the additional use of passive sensing requires particles to perform more averaging, which makes the phase transition from disorder to order emerge more smoothly. However, due to finite size of the domain for the simulated system, determining the location and nature of phase transition is difficult. A common tool to rigorously investigate this matter is finite size scaling analysis [43]. However, its implementation requires a large domain size to be simulated over a long period of time. Since our model is three dimensional, the number of particles is proportional to L^3, which makes employing finite size analysis infeasible due to computational demands. In [33], the nature of the phase transition as the sensing angle changes is detected as first-order in the two-dimensional case, however, for the three-dimensional model, a through investigation similar to the analysis in [22] is required, which is beyond the scope of this work. Being aware of the finite size effects, one can qualitatively describe the phase transition. Figure 3.5 shows the polarization time series for the case with no passive sensing stacked for 150 different values of sensing angle around the phase transition with resolution of 0.0035 radians, at $\eta_{\mathrm{a}} = 0.4$. When the sensing angle is less than critical value, polarization is uniformly low, and as this angle increases above a critical value, polarization is uniformly high. However, between these two unimodal states, the system sometimes converges to the ordered phase and if it does, the time it takes to reach the ordered phase is significantly longer than the transient as defined by our notion of stationarity. This can be a sign of the coexistence of ordered and disordered states, however, we failed to observe bimodality in contrast to what reported in two-dimensional model in [33]. In summary, whether the phase transition in the three-dimensional Vicsek model with no passive sensing is first-order and whether

implementing passive sensing will change the nature of phase transition requires a more thorough investigation which will be explored in future studies of this model.

3.5 Conclusion

Inspired by bats' active sensing and eavesdropping, a three-dimensional Vicsek-type model is introduced to study the effects of using active and passive sensing with restricted sensing angle on collective behavior of a group of individuals in the presence of noise. The range of parameters for which the ordered phase exists changes when passive sensing is introduced to the model. Also, at different values of active and passive noise amplitude, the maximum polarization happens at different sensing angles. Moreover, while the phase transition is sharp when only active sensing is implemented, it is noticeably smoother when passive sensing is added to the model.

Chapter 4

Tracking a Sound Source with Unknown Dynamics Using Bearing-Only Measurements Based on A Priori Information

The content of this chapter have appeared in the proceedings of the 2019 IEEE American Control Conference: Shirazi MJ, Abaid N. Tracking a Sound Source with Unknown Dynamics Using Bearing-Only Measurements Based on A Priori Information. In *2019 IEEE American Control Conference (ACC)*, 2019 Jul 10 (pp. 4491-4496).

4.1 Introduction

Sound source localization, which is also referred to as passive sonar, considers the challenge of estimating the location of a source of an incoming sound. Based on the wide range of research areas interested in the problem of sound source localization, it is hard to find the origin of this problem in the literature. Perhaps one of the first studies on this problem is a set of experiments performed by Rayleigh [44] to find out how humans can localize the source of a sound. This is still an active field of research in psychoacoustics, and summaries of new developments in this area can be found in [45],[46]. Biologists are also interested in sound localization since some animals such as bats and whales use sound to perceive their environment [4]. Although sound localization originated as a research question in biology, it finds many applications in engineering, especially in robotics. The more recent advances in sound source localization and its application in robotics can be found in [47] and [48].

The problem of sound source localization involves many challenges. Information about the location of the sound source is usually extracted through analysing the magnitude and the time of arrival of the sound to different sensors. Therefore, the first challenge is detecting the sound and estimating the delay in the reception time across receivers. Many signal processing techniques, such as generalized cross-correlation and eigenvalue decomposition along with different models for sound propagation and reverberation, are implemented to achieve this goal. A comprehensive review of these approaches is presented in [49].

After the sound signals are received and processed, the next step is extracting the direction of the incoming sound and the distance it traveled using different acoustic cues. Among these cues, the difference of the arrival time of the sound to each receiver, usually referred as Time Difference of Arrival (TDoA), is commonly used to estimate the sound direction [50, 51]. Finding sound direction is more challenging when only two receivers are used,

which mimics human localization (binaural localization). The complication in this case is due to geometrical symmetry called cone of confusion, or front-back confusion in the two dimensional case. This confusion can be resolved by breaking the symmetry using a head motion [52], or taking into account the acoustic shadow created by head defining a head model often referred as the Head Related Transfer Function (HRTF) [53, 54].

Range estimation, on the other hand, is a more challenging task in sound source localization and still is an active research area. In some approaches, the redundancy of several receivers is exploited to estimate the range of the sound source [50]. Another work estimates range using consecutive measurements as a head with a binaural sensor turns [55]. In indoor situations, some localization approaches take advantage of the reverberant sound energy to estimate the range [56]. The idea is that, while the energy of the sound signal received directly from the source depends on the distance between the source and sensor, the reverberated sound energy is independent of this distance. The work presented in [57] is another example of using environmental effects on the sound signal for localization by exploiting sound reflection and diffraction in an indoor environment.

Another approach in range estimation is to take advantage of sensor/source mobility by implementing some type of Bayesian estimation. In this approach, the localization problem essentially is a target tracking problem using a bearing-only sensor. The work represented in [58] employs a multiple mode Kalman filter to mitigate the effect of noise and uncertainty in tracking a moving sound source, but the authors assume the direct measurement of its location. They also assume three hypotheses for motion of the source–static, constant velocity, and constant acceleration–and based on Bayes' formula, estimate the probability of any of these assumptions. In [59], particle filtering is implemented to localize a moving sound source as the sensor is moving. In this work, the filter is designed assuming the sound source is stationary and then investigates what type of sensor motion will reduce the localization

error in the case of a moving sound source. The work presented in [60] considers localization of an intermittent moving sound source using a mixture Kalman filter. The location and speed of the sound source, as well as its activity status, are included in the state vector and therefore, a dynamic model is assumed for the motion of sound source and its activity.

As is briefly mentioned above, the sound localization algorithm based on Bayesian estimation assumes some dynamic model for the sound source to build transition probability. However, such a dynamic model may not always be available. Instead it may be possible to use some a priori information about the motion of the sound source. This information may come from our knowledge about the source. As an example, a beacon for guiding a group of vehicles using passive sonar may be designed to move with constant speed or generate sound with a specific pattern. This information can also be available through measurement, such as estimating speed based on the Doppler shift effect. This paper considers a case study to investigate the possibility of designing an estimator by exploiting a priori information combined with measurement data from a bearing-only sensor to perform sound localization.

4.2 Modeling

Consider the problem of localization of a sound source using a bearing-only sensor. As an example, a microphone array can be used as a bearing-only sensor that can measure the bearing angle of the incoming sound but not the range. The dynamics of the sound source is unknown but we know that the source is moving in the horizontal plane with constant speed v and it emits sound pulses at known intervals. Therefore, the measurement available to the sensor consists of the bearing angle of the incoming sound and the time the signal is received. To completely localize the sound source, an estimation algorithm is needed to extract the range of the sound source with respect to the sensor.

Although a dynamic model of the sound source is not available, it is possible to build up the dynamics and a measurement model using the existing information about its motion and the sensor measurement. To this end, the measurement vector is divided into two disjoint parts. The first part, which is referred to z^p, is used to build a dynamic model to predict the next state of the system. However, the second part of measurement vector, z^c, is used to build a measurement model to correct the prediction of states.

The time the sound reaches the sensor is related to the distance between the sound source and the sensor. When the time interval between pulses is known, it can be used to extract some information about the range of the source. If Δ is the time interval of the sound source and the kth signal is received at time t_k when the sound source is at range r_k, the next signal is expected at time t_{k+1} when the source is at range r_{k+1} and the following relation holds:

$$r_{k+1} = r_k + c\left(t_{k+1} - t_k - \Delta\right) + \nu_k, \tag{4.1}$$

where c is the speed of sound, and ν_k is the process noise, which is a zero-mean random variable independent from the states of the system which models uncertainties and measurement noise on reception time. In this model, it is assumed that the speed of the sound source is negligible compared to the speed of the sound, and therefore, when the signal is received, the sound source is approximately at the same location as when it emits the sound.

Fig. 4.1 shows a schematic of the motion of the sound source. The sensor is located at the origin and the localization goal is to estimate the range r. The sound source is moving on the dashed line in the direction of the arrows. When the sound source is at the point A at time step k, it emits a sound and then moves along the path to reach the point B at time step *k+1*, when it generates another sound. Since the speed of the source and the time interval between pulses are known, the distance the sound source has traveled during this time can

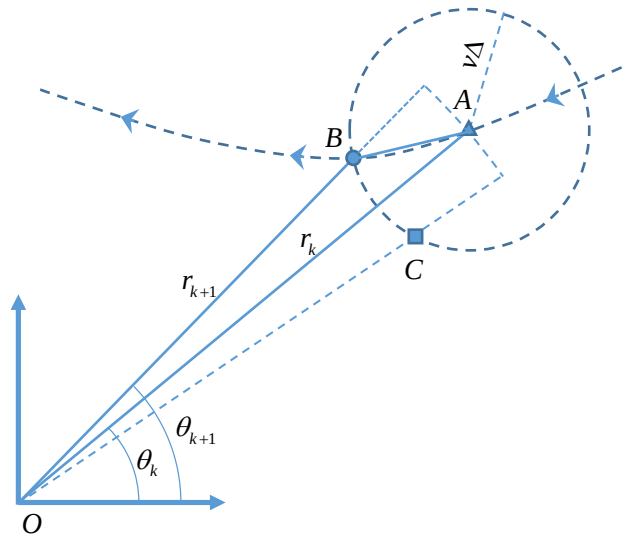

Figure 4.1: A schematic of the sound source moving in the plane with constant speed.

be approximated by $v\Delta$, assuming the path to be linear during this time period. Therefore, the location of point B is located on the circle with radius $v\Delta$ centered at A. Also, the range of B is known by (4.1), which reduces the possible location of the sound source at time step *k+1* to two points labeled as B and C in Fig. 4.1. Using the law of cosines in the triangle OAB gives us

$$(v\Delta)^2 = r_{k+1}^2 + r_k^2 - 2r_{k+1}r_k \cos(\theta_{k+1} - \theta_k). \tag{4.2}$$

where θ_k is the bearing of the sound source with respect to the sensor at time step k. Solving (4.2) for θ_{k+1} and then disturbing the result with a zero-mean independent noise ω_k leads to

$$\theta_{k+1} = \theta_k \pm \cos^{-1}\left(\frac{r_{k+1}^2 + r_k^2 - v^2\Delta^2}{2r_{k+1}r_k}\right) + \omega_k. \tag{4.3}$$

This equation shows the existence of two possible solutions for the triangulation as mentioned earlier (points B and C in Fig. 4.1). However, this confusion can be resolved when θ_{k+1} is measured by the sensor by choosing the sign that leads to closer value to the measured angle.

Although a model of the sound source motion is not available, using the known information about the sound source augmented with some measurement information (i.e. time), this method enables us to build up a dynamic model for the sound source as well as a measurement model of the remaining measurement vector (i.e. bearing angle) as expressed in (4.1) and (4.3), respectively. Now it is possible to apply a model-based estimation technique to find the range. To this end, in the following section, an estimator based on minimum mean squared error (MMSE) is presented. We comment that the strategy for the design of the estimator follows analogous logic to the classical proof of an extended Kalman filter (EKF), but must take into account our novel formulation that uses parts of the measurement for both prediction and correction [61].

4.3 Linear MMSE Estimation Algorithm

The dynamic model described in (4.1) can be expressed in the following format:

$$x_{k+1} = f\left(x_k, \nu_k; z_k^p, z_{k+1}^p\right), \tag{4.4}$$

where x_k and ν_k are state and process noise vectors. Also, z_k^p is the part of the measurement vector that is used for state prediction at time step k. It is important to note here that, since these measurements are available through the sensor, they are treated as a deterministic parameter while the state and process noise are stochastic variables.

The measurement model described in (4.3) can be expressed as

$$z_{k+1}^c = h\left(x_{k+1}, x_k; z_k^c\right) + \omega_k, \tag{4.5}$$

where z_k^c is the portion of the measurement vector used for correction of the predicted state

at time step k.

The goal of this section is to design an iterative estimator to find the range of the sound source. In other words, assuming that the state estimate at time step k, $\hat{x}_k$, is known and that all the measurements z_k^p, z_{k+1}^p, z_k^c, and z_{k+1}^c are available, it is desired to find an expression for $\hat{x}_{k+1}$.

Using the Taylor expansion about point $(\hat{x}_k, 0)$, one can linearize the dynamic model (4.4) to approximate x_{k+1} by

$$x_{k+1} = f\left(\hat{x}_k, 0; z_k^p, z_{k+1}^p\right) + F_k\left(x_k - \hat{x}_k\right) + \Gamma_k \nu_k, \tag{4.6}$$

where $F_k = \left.\frac{\partial f}{\partial x_k}\right|_{(\hat{x}_k,0)}$ and $\Gamma_k = \left.\frac{\partial f}{\partial \nu_k}\right|_{(\hat{x}_k,0)}$. The MMSE estimator returns the expected value of the posterior as the estimation. Therefore, the goal is to calculate

$$\hat{x}_{k+1} = E\left[x_{k+1} \middle| Z^{k+1}\right], \tag{4.7}$$

where Z^k is a notation to show all the measurements taken up to and including time step k, and $E[\cdot]$ is the expected value. Taking expected value from the linearized dynamics (4.6), and noting that ν_k is a zero-mean random variable and is independent from the states, one can find the expected value of the prior, or the predicted state as follows:

$$\bar{x}_{k+1} = E\left[x_{k+1} \middle| Z^k, z_{k+1}^p\right] = f\left(\hat{x}_k, 0; z_k^p, z_{k+1}^p\right). \tag{4.8}$$

The covariance of the prior distribution is defined as

$$\bar{P}_{xx} = E\left[\left(x_{k+1} - \bar{x}_{k+1}\right)\left(x_{k+1} - \bar{x}_{k+1}\right)^T \middle| Z^k\right]. \tag{4.9}$$

Substituting x_{k+1} and $\bar{x}_{k+1}$ from (4.6) and (4.8) into (4.9) yields

$$\bar{P}_{xx} = F_k P_{xx} F_k^T + \Gamma_k Q \Gamma_k^T \tag{4.10}$$

where P_{xx} is the covariance of the predicted state and Q is the covariance of the process noise. One can use the predicted state and the measurement model in (4.5) to find the predicted measurement at the next time step. The measurement model can be linearized about $(\bar{x}_{k+1}, \hat{x_k})$ to approximate z_{k+1}^c by

$$\begin{aligned} z_{k+1}^c &= h\left(\bar{x}_{k+1}, \hat{x}_k; z_k^c\right) \\ &\quad + \bar{H}_k \left(x_{k+1} - \bar{x}_{k+1}\right) + H_k \left(x_k - \hat{x}_k\right) + \omega_k, \end{aligned} \tag{4.11}$$

where $\bar{H}_k = \left.\frac{\partial h}{\partial x_{k+1}}\right|_{(\bar{x}_{k+1}, \hat{x}_k)}$ and $H_k = \left.\frac{\partial h}{\partial x_k}\right|_{(\bar{x}_{k+1}, \hat{x}_k)}$. Therefore, the predicted measurement can be found as the expected value of z_{k+1}^c. Using (4.11), and noting that the measurement noise is zero-mean and independent from the states, the expected measurement can be found as

$$\bar{z}_{k+1}^c = E\left[z_{k+1}^c \middle| Z^k\right] = h\left(\bar{x}_{k+1}, \hat{x_k}; z_k^c\right). \tag{4.12}$$

Using the linear MMSE estimator, the state estimate and its covariance can be found as [61]

$$\hat{x}_{k+1} = \bar{x}_{k+1} + \bar{P}_{xz} \bar{P}_{zz}^{-1} \left(z_{k+1}^c - \bar{z}_{k+1}^c\right), \tag{4.13}$$

$$P_{xx} = \bar{P}_{xx} - \bar{P}_{xz} \bar{P}_{zz}^{-1} \bar{P}_{xz}^T, \tag{4.14}$$

where $\bar{P}_{xz}$ is the covariance between predicted state and predicted measurement and $\bar{P}_{zz}$ is the predicted measurement covariance. To complete an iteration step, one needs to calculate

$\bar{P}_{xz}$ and $\bar{P}_{zz}$. Using the definition of the covariance,

$$\bar{P}_{xz} = E\left[\left(x_{k+1} - \bar{x}_{k+1}\right)\left(z^c_{k+1} - \bar{z}^c_{k+1}\right)^T \middle| Z^k, z^p_{k+1}\right]. \tag{4.15}$$

Substituting z^c_{k+1} and $\bar{z}^c_{k+1}$ respectively from (4.11), and (4.12) leads to

$$\begin{aligned}\bar{P}_{xz} &= E\left[\left(x_{k+1} - \bar{x}_{k+1}\right)\left(x_{k+1} - \bar{x}_{k+1}\right)^T \bar{H}^T_k \middle| Z^k, z^p_{k+1}\right] \\ &+ E\left[\left(x_{k+1} - \bar{x}_{k+1}\right)\left(x_k - \hat{x}_k\right)^T H^T_k \middle| Z^k, z^p_{k+1}\right] \\ &+ E\left[\left(x_{k+1} - \bar{x}_{k+1}\right)\omega^T_k \middle| Z^k, z^p_{k+1}\right].\end{aligned} \tag{4.16}$$

The last term in (4.16) vanishes since the measurement noise is assumed to be zero-mean and independent of the state variables. Substituting x_{k+1} and $\bar{x}_{k+1}$ from (4.6) and (4.8) into the second term in (4.16), leads to the following:

$$\bar{P}_{xz} = \bar{P}_{xx}\bar{H}^T_k + F_k P_{xx} H^T_k. \tag{4.17}$$

Similarly, one can calculate $\bar{P}_{zz}$ as follows

$$\begin{aligned}\bar{P}_{zz} &= E\left[\left(z^c_{k+1} - \bar{z}^c_{k+1}\right)\left(z^c_{k+1} - \bar{z}^c_{k+1}\right)^T \middle| Z^k, z^p_{k+1}\right] \\ &= E\left[\bar{H}_k\left(x_{k+1} - \bar{x}_{k+1}\right)\left(x_{k+1} - \bar{x}_{k+1}\right)^T \bar{H}^T_k \middle| Z^k, z^p_{k+1}\right] \\ &+ E\left[\bar{H}_k F_k\left(x_k - \hat{x}_k\right)\left(x_k - \hat{x}_k\right)^T H^T_k \middle| Z^k, z^p_{k+1}\right] \\ &+ E\left[H_k\left(x_k - \hat{x}_k\right)\left(x_k - \hat{x}_k\right)^T \bar{H}^T_k F^T_k \middle| Z^k, z^p_{k+1}\right] \\ &+ E\left[H_k\left(x_k - \hat{x}_k\right)\left(x_k - \hat{x}_k\right)^T H^T_k \middle| Z^k, z^p_{k+1}\right] + E\left[\omega\omega^T \middle| Z^k, z^p_{k+1}\right] \\ &= \bar{H}_k\bar{P}_{xx}\bar{H}^T_k + \bar{H}_k F_k P_{xx} H^T_k + H_k P_{xx}\bar{H}^T_k F^T_k + H_k P_{xx} H^T_k + R,\end{aligned} \tag{4.18}$$

where R is the covariance of the measurement noise. Again, the fact that the process and

measurement noises are zero-mean and independent from state variables is used to simplify the expression for $\bar{P}_{zz}$. Now it is possible to calculate the estimated state and its covariance for the next time step using (4.13) and (4.14), respectively. A summary of one iteration of the algorithm is presented in table 4.1.

The last step to finish the design of the estimator is to assume initial state and initial covariance. Similar to the EKF, this estimator operates based on linearization of the dynamic and measurement equations about the best estimate of the previous state. Therefore, the performance of the estimator strongly depends on how close the initial state estimation is to reality. This initial state and its covariance can be set using some a priori information about the initial state or through measurement. Here, we used a simple approach to get a rough estimate of source location. The change in bearing angle, $d\theta$, is measured by finding the difference between two consecutive bearing measurements. Then, assuming that the sound source is moving on a circular path, one can estimate the initial position to be

$$x_0 = \frac{v\Delta}{|d\theta|}, \tag{4.19}$$

and its variance is set to be equal to $v\Delta$, the amount that the sound source is moving between two pulses.

Finally, it is important to note a limitation of this approach. As it was mentioned before, the general idea of this localization approach is to use the measured time of arrival of the sound to predict its source's next location while using the bearing angle to correct the prediction, compensate the effect of noise, and improve localization confidence. However, when the sound source is moving radially toward or away from the sensor, there is no change in bearing angle and therefore implementing the correction step is out of the question. In fact, due to the existence of noise in the bearing angle measurement, the same problem occurs

when the change in angle is small compared to the standard deviation of the bearing angle measurement noise. In these situations, the measured bearing angle is dominantly noise and, if it is used for correction step, it may lead to divergence of the algorithm. Therefore, we used a metric similar to signal-to-noise ratio to evaluate the information in the measurement and skip the correction step when the signal is dominated by noise. If the change in bearing angle is shown by $d\theta$, we define this ratio ρ, measured in dB, as

$$\rho = 20 \log \frac{|d\theta|}{\sigma_\theta}, \tag{4.20}$$

where σ_θ is the standard deviation of the bearing angle measurement noise. This metric defines a bound around zero within which we assume the measurement is dominated by noise.

Table 4.1: An iteration of the estimation algorithm

Inputs: $\hat{x}_k, P_{xx}, z_k^p, z_{k+1}^p, z_k^c, z_{k+1}^c$
Outputs: $\hat{x}_{k+1}, P_{xx}$
Prediction:
$\bar{x}_{k+1} = f\left(\hat{x}_k, 0; z_k^p, z_{k+1}^p\right)$
$F_k = \left.\frac{\partial f}{\partial x_k}\right\|_{(\hat{x}_k,0)}, \Gamma_k = \left.\frac{\partial f}{\partial x_k}\right\|_{(\hat{x}_k,0)}$
$\bar{P}_{xx} = F_k P_{xx} F_k^T + \Gamma_k Q \Gamma_k^T$
Correction:
$\bar{z}_{k+1}^c = h\left(\bar{x}_{k+1}, \hat{x_k}; z_k^c\right)$
$H_k = \left.\frac{\partial h}{\partial x_k}\right\|_{(\bar{x}_{k+1},\hat{x}_k)}, \bar{H}_k = \left.\frac{\partial h}{\partial x_{k+1}}\right\|_{(\bar{x}_{k+1},\hat{x}_k)}$
$\bar{P}_{xz} = \bar{P}_{xx}\bar{H}_k^T + F_k P_{xx} H_k^T.$
$\bar{P}_{zz} = \bar{H}_k \bar{P}_{xx} \bar{H}_k^T + \bar{H}_k F_k P_{xx} H_k^T + H_k P_{xx} \bar{H}_k^T F_k^T + H_k P_{xx} H_k^T + R$
$\hat{x}_{k+1} = \bar{x}_{k+1} + \bar{P}_{xz}\bar{P}_{zz}^{-1}\left(z_{k+1}^c - \bar{z}_{k+1}^c\right)$
$P_{xx} = \bar{P}_{xx} - \bar{P}_{xz}\bar{P}_{zz}^{-1}\bar{P}_{xz}^T$
$k = k + 1$ and repeat

4.4 Simulation Results

To examine the performance of the proposed localization algorithm, numerical simulation is used. The sound source is moving with constant speed of 1 m/s in x-y plane. The bearing-only sensor is located at the origin and the bearing angle is measured from positive x-axis. The value of pulse intervals is set to be $\Delta = 0.2$ s and the variance of process noise is assumed to be $Q = 4 \times 10^{-4}$ m^2. The standard deviation of the measurement noise in sensing the bearing angle and time of arrival are respectively set to $\sigma_\theta = 0.005$ rad, and $\sigma_t = 0.1$ ms. Therefore the measurement noise covariance matrix is equal to $R = \text{diag}\,[(\sigma_\theta^2, \sigma_t^2)]$, where $\text{diag}\,[v]$ is a diagonal matrix in which the elements of vector v are located on the main diagonal.

Two different paths are considered for the sound source. In the first simulation, the sound source starts from point (1,1) and moves on a circle around the origin in the counter clockwise direction. Fig. 4.2 shows the actual (blue dashed line) and tracked (solid red line) paths of the sound source. Time series for the range estimation error, its covariance, and the change in measured bearing angle of sound source in this case are shown in Fig. 4.3. The red dashed lines show the bound when ρ is set to be 24 dB.

In the second simulation, the sound source is moving on a straight line. The simulation parameters are the same as mentioned in the first paragraph of this section. In this case, the sound source starts from (2,1) and moves horizontally to the left. The actual path and the estimated one are shown in Fig. 4.4. The range estimation error, estimation covariance, and the measured change in bearing angle for this case is shown in Fig. 4.5. Again, the red dashed lines show the bound when ρ is set to be 24 dB.

In order to investigate the robustness of the designed estimator, Monte Carlo simulations are performed for 100 repetition. The mean value of the range estimation error$\pm$ one standard

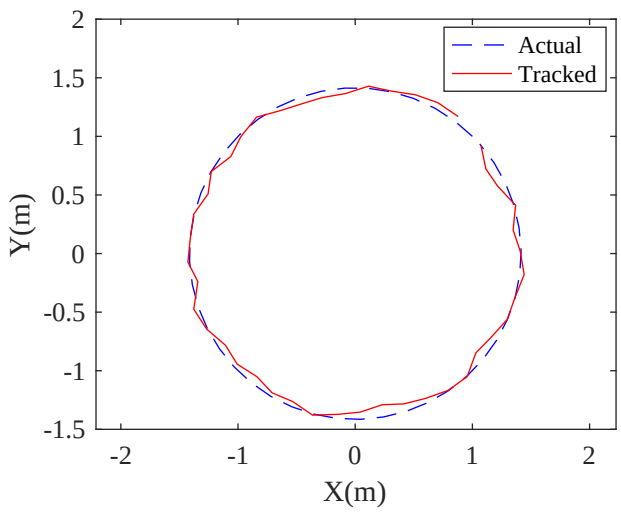

Figure 4.2: The actual path and the path tracked by the algorithm when the sound source moves on a circular, counter clockwise path around the sensor.

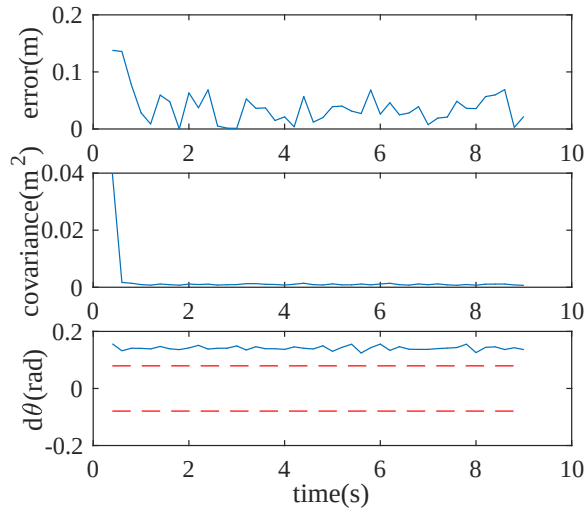

Figure 4.3: The range estimation error (top), its covariance (middle), and the change in measured bearing angle (bottom) of the sound source moving on a circular path around the sensor. The dashed red lines in the bottom plot show the bound when ρ is set to be 24 dB.

deviation for both paths are shown in Fig. 4.6.

4.5 Discussion

The algorithm developed in this work is the first of its kind, to the best of our knowledge, that uses part of a measurement for prediction within a standard Bayesian estimation procedure. As a result, we are able to use bearing-only measurements to track a sound source with unknown dynamics. The simulation results show that the algorithm can estimate the sound source location using the available information and measurement. In Fig. 4.2, the assumed initial range of the sound source is close to the actual value and the estimator can track the sound source in presence of process and measurement noise. Fig. 4.3 shows the performance of the estimator. The first plot shows range estimation error is relatively small although there

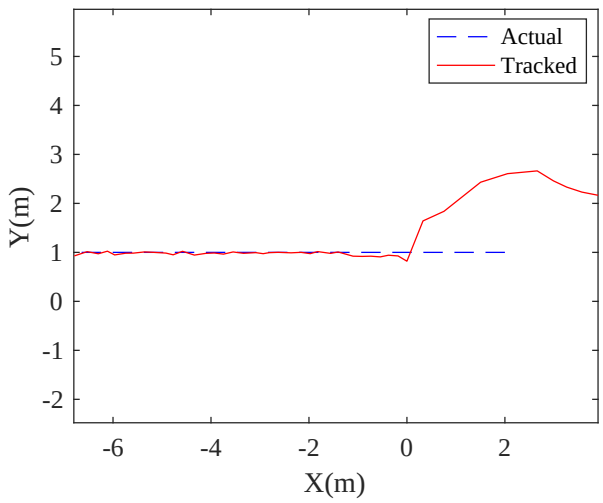

Figure 4.4: The actual path and the path tracked by the algorithm when the sound source moves on a linear path.

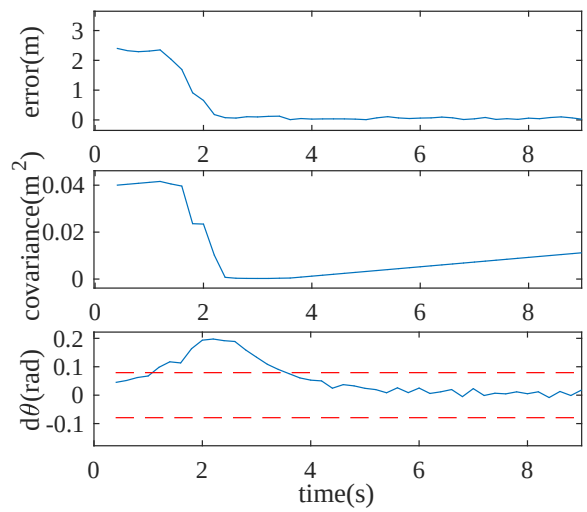

Figure 4.5: The range estimation error (top), its covariance (middle), and the change in measured bearing angle (bottom) of the sound source moving on a linear path. The dashed red lines in the bottom plot show the bound when ρ is set to be 24 dB.

are fluctuations due to the noise in the system. The covariance of estimation drops rapidly, which shows the confidence of the algorithm. This confidence can lead to inconsistency of the estimator mainly due to linearization, as it is well-known and studied for EKF [61]. The last plot shows that, in this example, the change in measured bearing angle is large compared to the noise standard deviation as it is outside the bounds set by ρ and therefore, these measurements are informative.

In the second case study, as it is shown in Fig. 4.4, the initial range estimation is relatively far from the actual state, but still the algorithm manages to converge. The first plot in Fig. 4.5 shows the range estimation error reduces to near zero. The estimation covariance decreases rapidly and then starts to increase. This increase in covariance happens when the change in bearing angle is perceived to be corrupted by noise, as the sound source moves away from the sensor at constant speed. Therefore the correction step is skipped and the

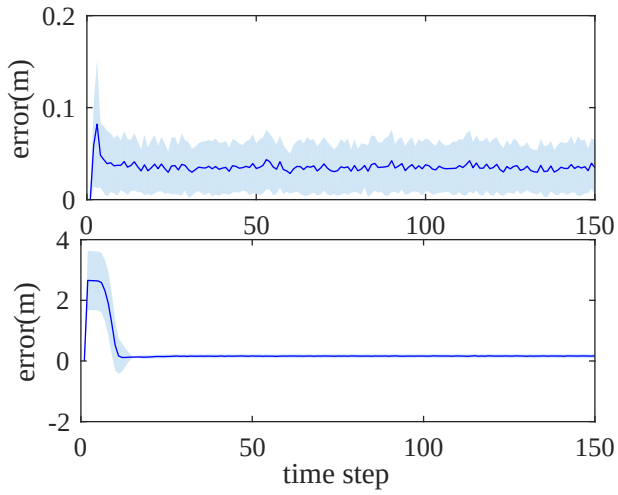

Figure 4.6: The mean value of the range estimation error over 100 Monte Carlo simulations for the circular path (above) and the linear path (below). Shaded region shows ± one standard deviation.

covariance increases due to noise accumulation. Finally, Monte Carlo simulations show that, given an initial state and noise covariances, the estimation algorithm results are robust over multiple runs.

4.6 Conclusions And Future Work

In this paper, the tracking problem of a moving sound source using a bearing-only sensor is studied when a dynamic model of the sound source is not available. Using information about its motion as well as some measurement information, a dynamic and measurement model is developed for the sound source. This model is used to predict the next location of the sound source and the remaining measurement information is exploited to correct this estimation. An EKF-type estimator is designed using MMSE estimation and its performance is studied using numerical simulation.

Although the simulation results show the convergence of the algorithm, there are still prac-

tical challenges in implementing the algorithm. The most important challenge is the limited range of operation which is related to use of bearing-only sensors. When the sound source is radially moving towards or away from the sensor, or when it is located far enough from the sensor that its bearing angle does not change significantly between two consequent pulses, the change in bearing angle is dominated by noise and implementing the correction update leads to bad estimates of the sound source location. This effect can be mitigated using accurate sensors, i.e. smaller noise covariance, which increases the cost in practical applications.

Another way to improve the performance of the algorithm even in higher noise covariance is to improve estimation of the initial range and its covariance. A more rigorous way to estimate initial state (compared to that used in this work) is to record a fixed amount of samples and use a smoothing algorithm to improve the initial estimation [61]. Since the success or failure of tracking depends on the accuracy of the estimation of the initial state and the parameters defining both the process and measurement noise, a parameter study to understand the dependency of the algorithm's success on these factors is necessary. These improvements are the main direction of our future work on this problem.

Chapter 5

Eavesdropping like a bat: toward fusing active and passive sonar for a case study in SLAM

The content of this chapter is ready to be submitted for possible publication in a peer-reviewed journal.

5.1 Introduction

Sensors are one of the integral components of any automated system responsible for providing information about the environment required for automation and control. Sensors can be categorized in two general groups, *passive sensors* and *active sensors*. Passive sensors passively detect the signals that are generated by a source in the environment. A camera used for object detection is an example of passive sensor, since it is only detecting and recording the light beams generated by a light source in the environment and reflected by the objects.

In contrast, active sensors actively spend energy to generate a signal and send it to the environment, and use the returning reflections for perception [3]. Sonar, lidar and radar are common examples of active sensors. Active sensors have an advantage over passive ones in that they can operate in environments not rich with the type of energy the sensor's receiver can detect. As an example, the practice of using a camera flash to capture images when the environment is dark changes the camera into an active sensor. In addition, active sensors may provide more information about the environment due to time difference between sending the signal and receiving the reflection, known as *time of flight* (ToF), which is simply not available to passive sensors. However, active sensors require an energy source to generate signals which can impose restrictions, especially on operation time. As another challenge specific to multi-agent applications, active sensors are prone to *signal jamming*, which refers to the confusion of the sensor to distinguish the reflection of its own signal from its peers'. This problem can be resolved by implementing a *matched filter* at the sensor's receiver to filter out any signal that does not match the signature of the sensor's own emitter signal through maximizing the signal to noise ratio [62].

In mobile robot applications, sonar is considered a particularly challenging sensor with limited success as compared to lidar and radar. Sonar sensors, which in this context are usually referred to as ultrasonic range finders, have slower data acquisition rates compared to lidar due to the difference between the speed of the sound and light. Therefore, when the robot has high velocity, the sensor will not be in the same nominal position at the transmitting and receiving times [63]. This can be modified if necessary by the approaches developed in bi-static sonar [64]. Moreover, in comparison with lidar, sonar has a wide beam width which makes it a less accurate ray-trace sensor with less angular resolution [65]. In addition, since sound has a fairly long wavelength (between 7 to 17 mm for a sound wave with frequency between 20kHz and 50kHz), most surfaces act as a mirror for sound. Therefore, when the

sound wave is not perpendicular to the surface, most of its energy specularly reflects away from the sensor or gets bounced back to sensor from another object, leading missed detection or wrong range detection [63, 65, 66, 67, 68, 69]. For example, a plane is only visible if the angle between the sonar axis and the normal vector to the plane is less than the opening angle of the main lobe of the beam [70]. One proposed solution to these missed reflections is to use a sonar ring to make a grid of sonar sensors to cover the entire body of the robot [71]. However, the collected data can be dramatically affected by vehicle orientation, for example, when the transducer is aligned with the node between the main and side lobes of the beam [63].

Another challenge regarding sonar sensors is their directionality, that is to say, the sonar is only able to view what is in front of it, within the main lobe (assuming that objects are rough or round enough to prevent specular reflection and yet can generate strong enough echoes). Although this may not be an important restriction in some applications such as obstacle avoidance, it can become critical in other tasks such as mapping or object classification [70]. One solution to this challenge is again the use of a sonar ring that emits sound waves in all directions. However, acoustic interference between neighboring transducers can impose challenges and limit the measurement sampling frequency which is not desirable in online applications [71, 72]. Another solution is to use a scanning sonar [63, 73], in which a single sonar sensor is reoriented to take multiple measurements from different vantage points. Having a wide beam width makes it hard to find the direction of an echo's return, as it is usually assumed the return is coming from the central axis of the sonar. We note though that in underwater sonars, which are more advanced than their in-air counterparts, the sophisticated design of the sonar head and beam forming techniques enables generation of narrow beams that leads to precise direction measurement. In addition to this limitation, scanning sonars suffer from slow update rate and therefore, the results are distorted by vehicle motion [63].

For example it takes at least 6 seconds for Tritech Miniking imaging sonar to complete a scan due to its mechanical limits and this time can increase dramatically depending on the range setting; at a 50 meter range setting, a complete scan need about 15 seconds [74]. In spite of all these challenges, sonar sensors are popular in mobile robot applications due to their cheap price [75]. In addition, sonar sensors are mostly used in underwater applications, since sound can travel further in comparison to radio waves and light. In the conductive sea water, radio waves attenuate fast and light suffers scattering [76]. These benefits of sonar make a strong case for their implementation in engineering applications.

In spite of all the challenges regarding the physics behind acoustics and sonar, some animals such as bats and dolphins demonstrate a successful use of sonar sensing in the nature. The implementation of sonar by animals, which is referred as *biosonar*, is intensively studied by researchers [4, 77]. Bat sonar involves only a transmitter, the larynx, and two ears as receivers, which is qualitatively different from the sonar rings and scanners mentioned above. However, bats are able to implement sonar in a very sophisticated way. They can balance sensor range, opening angle, and spatial resolution using techniques such as modulating sound frequency [39], temporal shape of the sound wave signal [40], or direction of the sound [41]. For example, bat foraging involves three phases: search, approach and terminal phase. Some bat species use lower frequency signals in the search mode, which provides wider opening angles and longer range due to less attenuation. When the target is detected in the approach phase, they use higher frequency signals to improve resolution and, in the terminal phase, they increase the call repetition frequency to get higher resolution of the prey location [4]. To create and analyse these acoustic signals, they may also use complicated motion in their nose leaves and pinnae , which has inspired engineers to build biomimetic emitters and receivers [78, 79, 80]. With two receivers, it is possible to find the direction of the sound source based on the time difference of arrival of the sound to two receivers. Time

difference of arrival is the fundamental principle of passive sonar, which is referred as binaural sound source localization when two receivers are used; this has been implemented in robotic applications [48]. A combination of binaural sound localization with active sonar range measurement leads to a sonar sensor that can measure range and bearing. Motivated by bat sensing, several research groups developed a sonar sensor based on this idea [81, 82, 83].

Studies on bat group behavior show other fascinating abilities of these animals that only manifest in group interaction. For example, it has been observed in the lab environment, when a pair of bats fly together, occasionally one bat stops making sounds presumably to avoid signal jamming [5]. How can a bat navigate and avoid obstacles without using its sonar? Another study performed in the field suggests that bats intentionally jam a peer's signal in competition over food [84]. Based on these studies, it seems that bats not only use their sonar actively, but also passively get information by *eavesdropping* on their peers' calls. In other words, bats are fusing the information they get through active and passive sonar to enhance their perception of the environment. This is not a common practice of sonar sensors in autonomous vehicle applications, which raises the research question of whether this type of information fusion can be beneficial in that context. In particular, can this type of eavesdropping behavior can be a solution to the limitations of sonar directionality by covering the *blind spot* of an active sensor with information from passive sonar? This may lead to the elimination of the slow update rate inherent in scanning sonar or sonar rings, especially since bats are not using any of the aforementioned approaches to deal with this limitation.

To investigate the possible benefits of fusing active and passive sonar, we investigate the canonical robotics problem of landmark-based Simultaneous Localization And Mapping (SLAM). In this problem, a robot explores an unknown environment to build a map by finding the location of landmarks in the environment and localizing itself within this map

simultaneously. We use a Monte Carlo numerical simulation and evaluate the performance of the algorithm in three different scenarios: (1) a robot using only active sonar with range and bearing measurements, (2) a robot using only passive sonar with bearing measurements, and (3) a robot fusing active and passive sonar. Different values of sensor opening and noise parameters are explored and the three scenarios are compared. The rest of the paper is organized as follows. In section II, we formally define the problem, provide simplifying assumptions, and describe the simulation scenarios. In section III, we introduce the dynamic model of the robot. Section IV describes the measurement models and the SLAM algorithm used in each sensing strategy. The simulation results are presented in section V and section VI is devoted to the concluding remarks and future work.

5.2 Problem Statement

In this section, we explain the simulation scenario and the simplifying assumptions made. A ground robot is located in an unknown environment that has unknown number of fixed point landmarks at unknown locations. The objective of the robot is to build a map of landmark locations and localize itself within the map. A beacon emits sound waves in the environment at a known fixed frequency, which will be reflected by the landmarks. We assume that the robot can receive the echos of the beacon's sound reflected from the landmarks. This assumption is idealized in general since, in real scenarios, the landmark may specularly reflect the sound and the echo may not be able to be received from some directions, or the robot may be located in the acoustic shadow of the landmark and may not receive any signal. However, in a convex environment such as indoor applications with round landmarks or landmarks with rough surfaces that defuse the incident sound from the beacon, this assumption may be valid.

The ground robot is assumed to be equipped with a sonar emitter that can emit a sound at a different frequency than the beacon. Therefore, at the receiver, the robot can distinguish whether the received signal is a reflection of the beacon or its own emitter. The robot is able to measure the range to the landmark located within the region defined by its sensor opening, which is the angular range of the robot's receiver. Again, we assume that the specular reflection does not prevent the sensor from missing the echo. Also, it is assumed that the robot uses more than one receiver and is thus able to measure the bearing angle of the incident sound in a single measurement. With two receivers, it is possible to localize the bearing angle to the sound source by calculating time difference of arrival of the incident sound to the receivers, up to a cone– known as the cone of confusion– whose axis passes through both receivers. In two dimensions, the cone of confusion reduces to ambiguity between two points, one in the front and the other in the back of the receivers, which is referred as front-back confusion [53]. There are several ways to resolve this confusion such as: using consecutive measurements and performing probabilistic hypothesis testing [60, 85], implementing a head motion between two consecutive measurements to break symmetry [52], or exploiting the difference in frequency response of the receiver at different directions, usually referred as *head related transfer function* (HRTF) in the acoustic and biology community studying human and animal in the context of binaural sound localization [54, 86]. If the robot uses an array of at least three receivers, it can calculate the direction of the incident sound without any confusion [51], which is what we assume for this work.

Finally, the robot is assumed to be able to detect the echo of the beacon's sound reflected from the nearby landmarks. This is the situation in our inspiring system of eavesdropping bats where two bats are flying close by and one of them acts as a beacon for the other bat. Therefore, one way to create such a situation is to make the beacon follow the robot. We can also assume that the environment is uniformly sonified by several beacons. This assumption

is analogous to uniform lighting of the environment for the use of a camera.

The robot can operate in three different modes to solve the SLAM problem. In the first mode, the robot only detects the echo of its own emitter reflected from the environment and filters everything else, including the echoes generated by the beacon. We refer to this mode as *active SLAM*, which is the way current sonar sensors are implemented [63]. In this mode, the robot will have access to range and bearing measurements of all the landmarks located in the range of the emitter within its main lobe. In the second mode, the robot does not emit any signal and only uses the echoes of beacon's sound. We call this mode *passive SLAM*. Because the robot lacks range information, it can only measure the bearing angle of the incident sound by comparing time difference of arrival between its receivers. In this way, it is similar to the bearing-only SLAM problem studied in the literature, for example, [87]. Finally, in the third mode, the robot uses its emitter and detects its echoes from landmarks as well as the echoes of the beacon's sound. In this case, the robot will have access to the range and bearing information of the actively located landmarks which are within the main lobe of the robot's emitter. For other landmarks detected passively through the beacon's echo, the robot will have access to range information only. This mode, which is a combination of active and passive sensing, resembles the eavesdropping behavior observed in bats. We refer to this mode as the *fused SLAM*.

In light of bat eavesdropping, the main research question of this work is whether combining active and passive sonar can be beneficial for SLAM. To this end, we compare the robot's performance when it is acting in active, passive, and fused modes and we perform a sensitivity analysis over the range of parameters using Monte Carlo simulations. Showing that fused sensing can benefit SLAM may open a new paradigm for sonar implementation in canonical engineering problems. In the next section, we present a simplified model of the robot motion and different sensing modes.

5.3 Modeling

Here, we assume a simple model for the robot, in which its motion can be determined by its translational and rotational velocities,

$$\begin{aligned} x^r_{k+1} &= x^r_k - \frac{v_k}{w_k}\sin(\phi_k) + \frac{v_k}{w_k}\sin(\phi_k + w_k dt) + \nu^x_k, \\ y^r_{k+1} &= y^r_k - \frac{v_k}{w_k}\cos(\phi_k) + \frac{v_k}{w_k}\cos(\phi_k + w_k dt) + \nu^y_k, \\ \phi_{k+1} &= \phi_k + w_k dt + \nu^\phi_k, \end{aligned} \tag{5.1}$$

where x^r_k, y^r_k, and ϕ_k are respectively the x, y coordinates and orientation of the robot, v_k and w_k are respectively the translational and rotational velocities, and ν^x_k, ν^y_k, ν^ϕ_k are the corresponding components of the process noise vector sampled from a Gaussian distribution with covariance $\mathbf{Q}_k$, and dt is the discretization time step.

The robot can only sense the sound if the sound source is located within a range R of the robot, and inside a circular section with opening angle α, modeling the main lobe of the sonar's emitter. We assume the receivers are omni-directional and therefore, the bearing angle of the sound source can be measured omni-directionally. Thus, the passive sonar is able to measure the bearing angle of the sound source or a reflector as long as it is located within the range R from the robot. A schematic of different sensing mechanisms is illustrated in figure 5.1.

5.4 EKF-SLAM

As mentioned before, we tackle the landmark-based SLAM problem. Among all the methods developed to solve the SLAM problem, we use the approach based on Extended Kalman

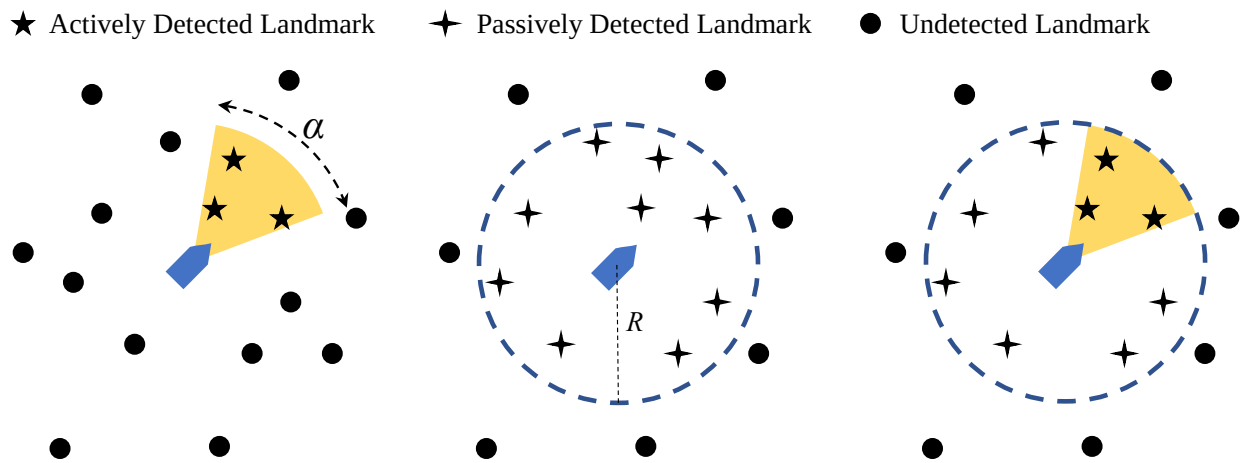

Figure 5.1: A schematic figure of different sensing strategies. Active sonar (left) provides range and bearing information of the landmarks located within sensor opening α. Passive sonar (middle) can only measure bearing angle omni-directionally if the landmark is located within some distant R of the sensor. Fused active and passive sonar (right) measures range and bearing to the landmarks within the sensor's opening α and the bearing to other landmarks within distance R.

Filter, i.e. EKF-SLAM, for several reasons. The EKF-SLAM is the most fundamental algorithm to solve SLAM. Also, this algorithm is relatively computationally cheap, especially for small maps where the covariance matrices are small. This makes it easier to perform Monte Carlo simulations to compare the performance of different measurement strategies. Finally, the performance of the the EKF algorithm is affected by the availability of new measurements. Since this algorithm is based on linearization about the best estimate of the states, we expect this algorithm will be able to clarify the differences between different sensing strategies.

In the two dimensional landmark-based SLAM, the state vector contains the location and orientation of the robot as well as the locations of landmarks. Since we assume the landmarks are stationary, the only changing part of the dynamics equation corresponds to the robot and is stated in equation (5.1). We assume that the data association is known for the sake of simplicity of comparing performance of using different sensing approaches. Assuming

known association is common in bearing only SLAM using camera, based on the color or other features of the landmarks [88, 89, 90]. However, based on current state of the art, it is more challenging to extract acoustic features of the reflector from the received echo, even though bats appear to be able to deal with challenge. A recent study shows the effectiveness of using artificial sonar reflectors inspired by floral shapes in reducing ambiguity is using sonar sensors through generating distinguishable reflections [91]. In addition, there are general techniques for data association such as use of Mahalanobis distance [92] and joint probabilistic data association (JPDA) [93]. In the bearing-only SLAM, the data association is more challenging since the location of landmarks cannot be found by a single measurement. Several algorithms are suggested to solve data association, such as data association based on clustering without using any feature information [94], or a combination of hypothesis testing and some feature information such as [95] and [96].

In the following sections, we briefly summarize the EKF-SLAM algorithm using active sonar, passive sonar, and fusion of these sensing approaches.

5.4.1 EKF-SLAM with active sonar

As stated before, while using active sensing, the robot has access to range and bearing information of each landmark within the circular segment of sensing and EKF-SLAM is one of the most common algorithms using range and bearing measurement [92]. In this case, the measurement vector, $\mathbf{z}_k$, is the augmentation of the range and bearing measurement $\mathbf{z}_k^j$ from all landmarks j in the sensing region:

$$\mathbf{z}_k^j = \begin{bmatrix} \sqrt{\delta x^2 + \delta y^2} \\ \arctan\left(\frac{\delta y}{\delta x}\right) - \phi_k \end{bmatrix} + \omega_k, \tag{5.2}$$

where δx and δy are the horizontal and vertical distances between the robot and the jth landmark, respectively, and ω_k denotes the measurement vector noise sampled from a Gaussian distribution with covariance $\mathbf{R}_k$. This equation is obtained by using the geometric relation between robot and landmark location and the range and bearing measurement and solving it for the range and bearing values. Since active sonar can provide both range and bearing, this equation can be solved with even one measurement sample. Therefore, only one measurement is sufficient to initialize the location of the landmark.

If $\hat{\mathbf{x}}_k$ denotes the estimation of the state vector at time step k and $\mathbf{P}_k$ is its covariance, the state estimation vector and its covariance at the next time step can be found by

$$\begin{aligned} \hat{\mathbf{x}}_{k+1} &= \bar{\mathbf{x}}_{k+1} + \bar{\mathbf{P}}_{xz}\bar{\mathbf{P}}_{zz}^{-1}\left(\mathbf{z}_{k+1} - \bar{\mathbf{z}}_{\mathbf{k+1}}\right), \\ \mathbf{P}_{k+1} &= \bar{\mathbf{P}}_{k+1} - \bar{\mathbf{P}}_{xz}\bar{\mathbf{P}}_{zz}^{-1}\bar{\mathbf{P}}_{xz}^{T}, \end{aligned} \tag{5.3}$$

where $\bar{\mathbf{x}}_{k+1}$ and $\bar{\mathbf{P}}_{k+1}$ are respectively the predicted state and its covariance, $\bar{\mathbf{z}}_{k+1}$ is the predicted measurement which is an augmentation of predicted measurement of each landmark as calculated in equation (5.2) and $\bar{\mathbf{P}}_{zz}$ is the augmented measurement covariance containing the sensor noise covariances for each landmark measurement. Finally, $\bar{\mathbf{P}}_{xz}$ is the predicted covariance of measurement with state, and $\hat{\mathbf{x}}_{k+1}$ and $\mathbf{P}_{k+1}$ are the estimated state and its covariance at time step $k+1$, respectively. More detail on calculation of the extended Kalman filter can be found in [61].

5.4.2 EKF-SLAM with passive sonar

In contrast to active sonar, the passive sonar does not have access to the range measurement and therefore, only the bearing angle measurement is accessible. In this case, the

measurement equation is

$$\mathbf{z}_k^j = \arctan\left(\frac{\delta y}{\delta x}\right) - \phi_k + \omega_k, \tag{5.4}$$

where δx and δy are the horizontal and vertical distances between the robot and the jth landmark, respectively, and ω_k denotes the bearing angle measurement noise sampled from a Gaussian distribution with variance $\sigma_{\theta k}^2$.

Since the passive sonar is a bearing-only sensor, the location of a landmark cannot be estimated using one single measurement and therefore, equation (5.4) cannot be used to find the predicted measurement $\bar{\mathbf{z}}_{\mathbf{k+1}}$. Thus, it is necessary to initialize the landmark location before performing the extended Kalman filter. This is a challenge in performing bearing-only SLAM, and several solutions have been presented in the literature. A good summary and comparison of these methods is presented in [97]. We use the method introduced in [94]. In this approach, the landmark location is represented by a Gaussian distribution in the plane. The center of this distribution is defined as the intersection of bearing direction lines measured from two different robot positions. Knowing the center point of the distribution from each robot location, the covariance of the location of the landmark can be estimated assuming a large range covariance and using the bearing angle measurement noise covariance, and then applying the appropriate change of coordinate and translating the covariance of the robot location, based on the method derived in [98]. Finally, the covariance of the landmark location can be found by fusing the covariance matrices estimated from each of the different robot locations. Since the initialization accuracy improves when the apex angle formed between two robot locations and landmark is large, we only start initiating a landmark after detecting it passively in 5 consecutive measurements, using the first and last robot locations for initialization.

After each landmark is initialized, the landmark location and its covariance is augmented in the state vector and the covariance matrix to perform one step of Kalman filter estimation

according to equation (5.3) with associated measurement values. We should note here that in augmenting the covariance of the new landmark to the state covariance matrix, we follow the approach in [94], in which we simply add the landmark covariance as a diagonal term to the state covariance matrix to ensure that the state covariance remains positive definite. In other words, we assume that the uncertainty of the newly detected landmark is independent from the uncertainty of the other landmarks. However, this assumption is not accurate since the landmark covariances are coupled through the robot location. However, this assumption is not detrimental to the entire estimation process since it is only applied in initialization steps and the strength of this coupling emerges in the future iterations of the EKF algorithm.

5.4.3 EKF-SLAM fused sonar

The active sonar has the advantage of range measurement while passive sonar has the advantage of being omnidirectional. The motivation behind combining the active and passive sonar measurement is to exploit the advantages of the two measurement approaches to improve performance of the robot. This combination resembles eavesdropping that may be used by bats during their group flight; however, is it has not been implemented along with active sonar in robotic systems to the best of our knowledge.

In this mode, the robot has access to the range and bearing measurement of the landmarks located within the active sonar beam pattern, which is modeled by a circular sector, as well as the bearing measurement from landmarks within ranging distances through passive sonar. Therefore, the measurement equation is the augmentation of the measurement equations of the active sonar and passive sonar presented in equations (5.2) and (5.4), respectively. The landmarks that are detected using passive sonar are initialized through the same process explained in the previous section. When the state vector and its covariance become available,

we can perform an EKF update as presented in equation (5.3).

5.5 Simulation results

5.5.1 Simulation setup

To evaluate the performance of the different sensing strategies for different parameter values, we performed numerical simulation. The robot is placed in an environment with a regular rectangular array of landmarks with horizontal and vertical distances of 1 and 2 meters, respectively. The array is large enough that the robot will never reach the boundary of array during simulation time. This is in essence similar to the control volume approach commonly used in fluid mechanics and collective behavior analysis. This way, in all simulation conditions, the robot explores an area with constant density of landmarks by being away from the edges of the landmark array. Therefore, simulation results will not be affected by the density of landmark in the environment.

Since there are random parameters in the system, we perform a Monte Carlo simulation of 1000 repetitions. The initial location of the robot is selected randomly with uniform density within a box around the central landmark, such that the closest landmark to each point in the box is the central landmark. Therefore, within a large grid of landmarks that contains the robot during the simulation time, this selection of initial conditions samples from all possible cases within the entire grid. In addition, the initial orientation of the robot is also selected randomly from a uniform distribution between 0 and 2π radians. Figure 5.2 shows a sample snapshot of the simulation.

The parameters used in these simulations are related to either the robot or the sensor. The robot parameters are the translational speed v_k, rotational speed w_k, standard deviations

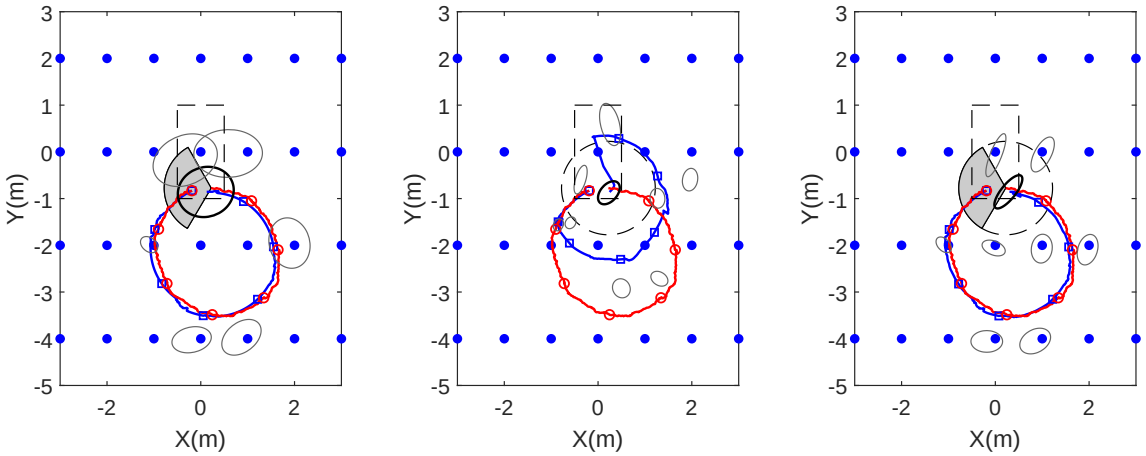

(a) Active sonar (b) Passive sonar (c) Fused sonar

Figure 5.2: A snapshot of the simulation. The paths in the left, middle, and right figures are associated with the EKF-SLAM solution when the robot is using active sonar, passive sonar, and fused sonar, respectively. The shaded circular sector centered at the robot location shows the opening angle of the active sensing, which only presented in active and fused sonar cases. The dashed circle centered around the robot shows the region where robot can sense using passive sonar. The dashed rectangle at the origin shows the region where the initial location of the robot is sampled uniformly from in each Monte Carlo simulation. The grid of blue circles show the landmarks presented in the environment. The red paths with circular markers is the real path the robot is taking, which is identical in all three cases. The blue paths with rectangular markers are the estimated path of the robot found through localization. The confidence region of the robot position is shown by the solid black ellipse around robot's estimated location. The confidence region of landmark estimation is shown with gray ellipses, where the estimated landmark location are at the centers.

of the robot's horizontal and vertical position noises and rotational noise. The sensor parameters are standard deviations of range and bearing measurement noises and the opening angle of the active sonar. All the noise values are assumed to have a zero mean Gaussian distribution.

In order to perform a fair comparison, in each Monte Carlo simulation, the robot parameters, initial condition, and process noise realizations are set to be identical between different sensing strategies. Also, since the bearing measurement in all strategies uses the time difference of arrival, the bearing measurement noise realization is considered to be identical in all

Table 5.1: Simulation parameters

Variable	**Symbol**	**Value**
Time step	Δt	1/10 s
Translational speed	v_k	0.2 m/s
Rotational speed	w_k	0.15 rad/s
Number of landmarks	-	81
Number of repetitions	N	1000
Standard deviation of robot's x, y position noise	σ_x, σ_y	0.01 m
Standard deviation of robot's orientation noise	σ_ϕ	0.0075 rad
Sensing range	R	1 m
Active sonar opening angle	α	$[\frac{\pi}{10}, 2\pi]$
Standard deviation of range measurement noise	σ_r	0.01 m
Standard deviation of bearing angle measurement noise	σ_θ	$[\frac{\pi}{900}, \frac{\pi}{6}]$
Total time steps in averaging window	K	600

cases. In addition, the range measurement noise realization is set to be equal in the active and fused sensing strategies. To compare the effectiveness of different strategies, we performed simulations for different values of standard deviation of bearing measurement noise and active sonar opening angle, while keeping the accuracy of range measurement constant.

Since the translational and rotational speed of the robot is assumed to be constant, the robot tries to move on a circle but the actual path is not a perfect circle due to the process noise. The simulation stops if the robot does not detect a new landmark for 600 time steps, which is more than the time required for the robot to close the loop. Table 5.1 summarizes the numerical values of all parameters used in numerical simulation.

5.5.2 Metrics

In this section, we evaluate the performance of EKF-SLAM using different sensing strategies. To this end, we compare the simulation results to answer three general questions: which strategy reports more information about the landmarks in the environment, which strategy

estimates the robot location more accurately, and finally, which strategy does a more accurate estimation of its state vector during the final stage of the simulation. In the following, we define metrics to evaluate these performance criteria. Each metric is evaluated for all the Monte Carlo simulations and their average is used for comparison.

As it is mentioned before, the robot terminates its operation when it does not detect a new landmark for 600 time steps. Therefore, the termination time, $K_{\max}$, can be different and can be used as a metric of how quickly the robot can scan the environment. In addition, the number of landmarks that a robot can report at the end of simulation, $N_{\max}$, is also an important metric on how effectively the robot can scan the environment. We use these two metrics to evaluate the effectiveness of different sensing strategies to explore the environment.

In order to evaluate the accuracy of different sensing strategies in localizing the robot, we use the truth model to calculate the least squared errors in the robot's location and its heading angle, calculated over the window of the last 600 time steps. In other words, for robot location, we calculate

$$\Delta\rho = \sqrt{\frac{\sum_{k=K_{\max}-N_w+1}^{K_{\max}} \left[\left(\hat{x}_k^r - x_k^r\right)^2 + \left(\hat{y}_k^r - y_k^r\right)^2 \right]}{N_w}}, \tag{5.5}$$

where $\Delta\rho$ is the root mean squared error (RMSE) in robot's location, $\hat{x}_k^r$ and $\hat{y}_k^r$ are the estimated two-dimensional coordinates of the robot location at time step k, respectively. The true location of robot at time step k is known through the truth model to be equal to x_k^r and y_k^r. The simulation length is $K_{\max}$ and N_w denotes the length of the averaging window, which is set to be 600 time steps. Similarly, for robot's heading, we find

$$\Delta\phi = \sqrt{\frac{\sum_{k=K_{\max}-N_w+1}^{K_{\max}} \left(\hat{\phi}_k - \phi_k\right)^2}{N_w}}, \tag{5.6}$$

where $\Delta\phi$ is the root mean squared error in robot's heading, $\hat{\phi}_k$ and ϕ_k are estimated and the true values of the robot's heading at time step k, respectively.

Finally, we compare the performance of the EKF using different sensing strategies in estimating the associated state vector. Since the number of landmarks detected by different sensing strategies can be different, to make a fair comparison, we only include the landmarks that have been detected by all the sensing strategies into the state vector. We use is the root mean squared error of state vector over the averaging window

$$\Delta\mathbf{x} = \sqrt{\frac{\sum_{k=K_{\max}-N_w+1}^{K_{\max}} \|\hat{\mathbf{x}}_k - \mathbf{x}_k\|^2}{N_w}}, \tag{5.7}$$

where $\hat{\mathbf{x}}_k$ and $\mathbf{x}_k$ are the estimated state and the true state at time step k, respectively. In addition to accuracy of estimation, we also evaluate the confidence of the estimation by calculating the maximum eigenvalue of the covariance matrices, as well as the Frobenius norm of the covariance matrix calculated by the EKF in different sensing strategies.

Finally, we evaluate the consistency of the estimation using different sensing strategies by the chi-squared filter performance metric [61]. First, we calculate the Normalized Estimation Error Squared (NEES) at each time step,

$$\chi_k = (\hat{\mathbf{x}}_k - \mathbf{x}_k)^T \mathbf{P}_k^{-1} (\hat{\mathbf{x}}_k - \mathbf{x}_k). \tag{5.8}$$

If the filter is consistent, then the estimation error becomes a sample from a zero mean distribution with covariance $\mathbf{P}_k$. Therefore, the NEES calculated in (5.8) should be a sample from a chi-squared distribution of degree equal to the degree of the state vector. Otherwise, the covariance $\mathbf{P}_k$ reported by the EKF is not a good representative of the actual covariance of the estimation. Therefore, it is possible to evaluate the consistency of the filter by counting

the number of simulations that the NEES calculated by (5.8) deviates from the statistics of chi-squared distribution, given an acceptable deviation region. If too many cases deviate from the chi-squared distribution, the estimation covariance is not a good representative of the true accuracy of the filter. It is a well known disadvantage of the EKF that it tends to face consistency issues and be over confident; in other words, the filter reports a wrong estimate of the state vector with small confidence regions [99]. This metric is designed to identify those errors if they occur.

5.5.3 Results

The simulation results are presented in this section. We report: the RMSE in robot localization, the maximum number of detected landmarks during the simulation time, the RMSE of the location of landmarks detected by all the sensing scenarios, the maximum eigenvalue of the state estimation error covariance, and the chi-squared consistency test of the state estimation.

Robot localization accuracy: The RMSE in robot's location is shown in figure 5.3, when the robot only uses active sonar (figure 5.3 (a)), only uses passive sonar (figure 5.3 (b)), and when it fuses active and passive sonar (figure 5.3 (c)). We can see from this figure that, when the robot only uses active sonar with a constant opening angle, the robot localization error increases as covariance of bearing angle measurement increases. At constant covariance of the bearing angle measurement noise, the error decreases as the opening angle increases and the rate of change of error is higher in smaller opening angles.

As it is shown in figure 5.3 (b), when the robot only uses passive sonar, the error in the robot's location is approximately constant for each opening angle, but the error is larger for very small bearing measurement noise covariance.

Finally, figure 5.3 (c) shows that, when the robot fuses the information of active and passive sonar, the error in the robot's location is almost always smaller in magnitude compared to when it only relies on active sonar for all values of α and σ_θ. In contrast, comparison of fused sonar and passive sonar scenarios shows that the error in robot's location is only smaller in fused sonar for the very small values of σ_θ. The RMSE of robot's heading angle for different sensing strategies shows a similar pattern as shown in figure 5.4.

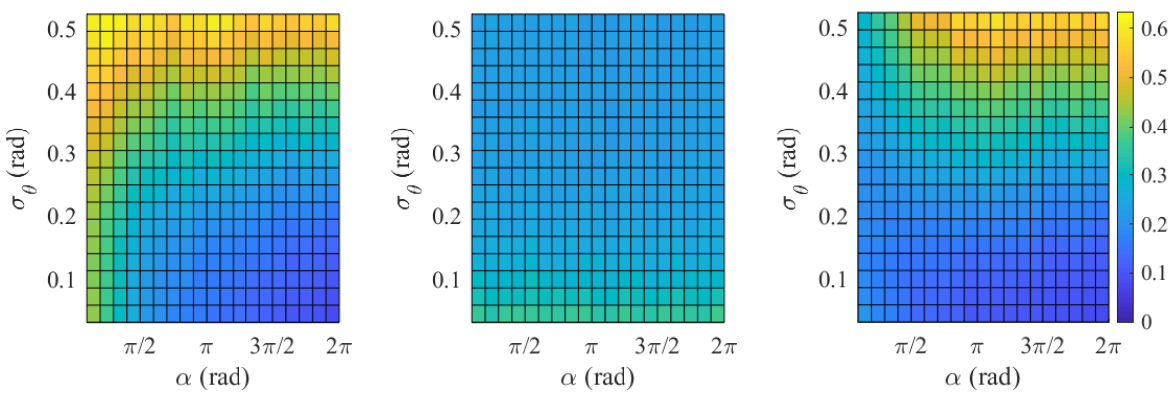

(a) Active sonar (b) Passive sonar (c) Fused sonar

Figure 5.3: RMSE of the robot location for (a) active sonar, (b) passive sonar, and (c) fused sonar.

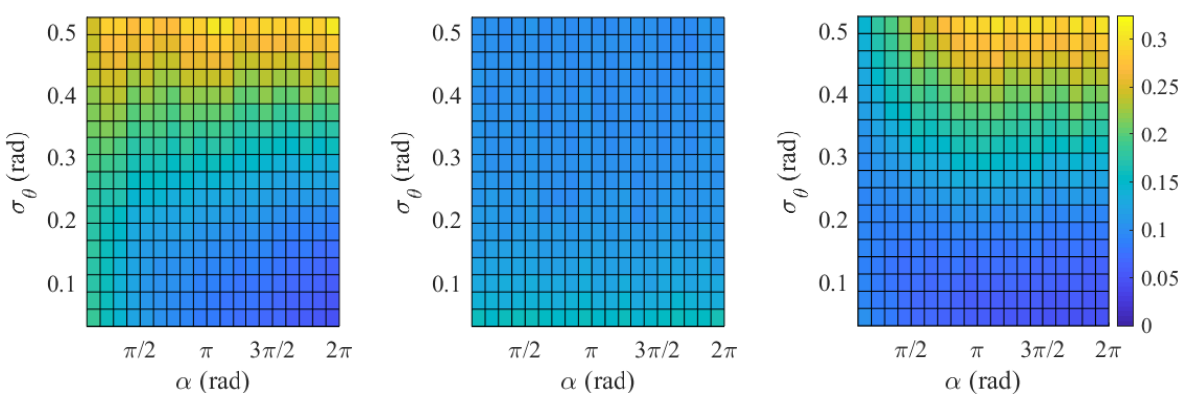

(a) Active sonar (b) Passive sonar (c) Fused sonar

Figure 5.4: RMSE of the robot heading for (a) active sonar, (b) passive sonar, and (c) fused sonar.

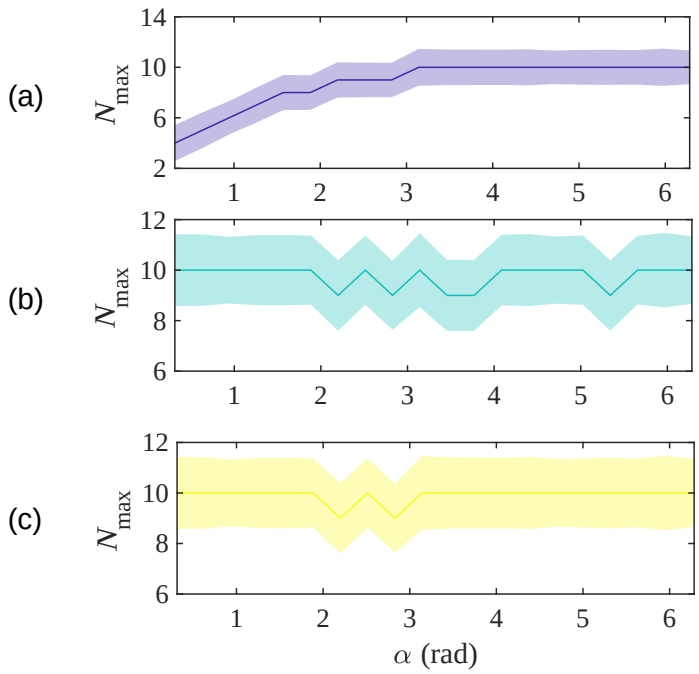

Figure 5.5: Maximum number of landmarks detected by (a) active sonar, (b) passive sonar, and (c) fused sonar. The lines show the mean over the Monte Carlo simulations and the shaded area shows ± one standard deviation

Landmark detection: As mentioned before, the robot terminates its search when it does not detect a new landmark for 600 time steps, and we denote the number of time steps it takes for the robot to finish its search by $K_{\max}$. The simulation results show that using different sensing strategies does not make a significant difference between them. However, as it is shown in figure 5.5, the number of detected landmarks shows that $N_{\max}$ is less by up to a factor of 3 when active sensing with small opening angles are used compared to passive or fused sensing.

State estimation: The RMSE in localization of the landmarks detected by all the sensing mechanisms is shown in figure 5.6. This plot shows the same general pattern of the RMSE in robot localization as shown in figure 5.3. In the active and fused sonar cases, the RMSE value increases as the opening angle increases at a constant σ_θ. This error also increases as

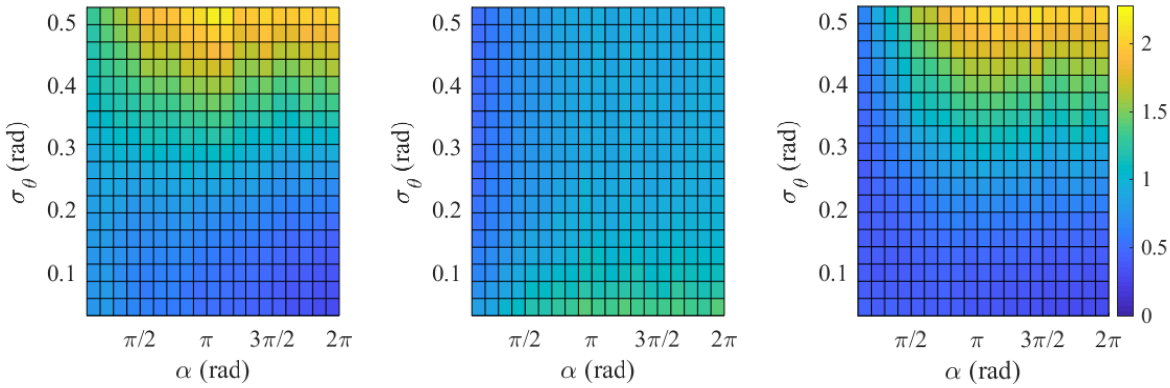

(a) Active sonar (b) Passive sonar (c) Fused sonar

Figure 5.6: RMSE of the estimated location of the landmarks detected by all sensing mechanisms for (a) active sonar, (b) passive sonar, and (c) fused sonar.

σ_θ increases at a constant opening angle. In passive sonar case, the RMSE is almost constant but it is relatively smaller for very small values of opening angle α and is relatively larger for very small values of σ_θ.

Figure 5.7 shows the maximum eigenvalue of the estimation error covariance for different sensing strategies. For active sonar, the maximum eigenvalue of the estimation error covariance gets smaller as the opening angle increases, but it is approximately constant as the bearing angle measurement noise changes. This metric is significantly higher in passive sonar, especially for higher values of σ_θ. Fused sonar is similar to active sonar except for small opening angle and significant σ_θ, which shows higher values in comparison to active sonar, and for small σ_θ and opening angles less than π, which shows smaller values. Also for each parameter, the value of this metric in fused sonar is always less than or equal to its corresponding value in passive sonar.

The results of the chi-squared test is shown in figure 5.8. This metric is more or less equivalent in active and fused sonar, except for very small values of opening angle and σ_θ, where active sonar shows smaller values. The chi-squared test value decreases monotonically for passive

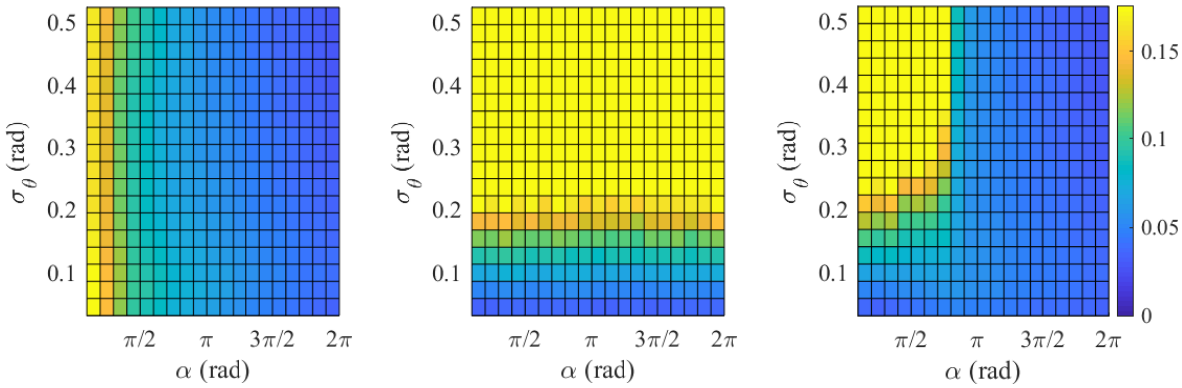

(a) Active sonar (b) Passive sonar (c) Fused sonar

Figure 5.7: Maximum eigenvalue of the state estimation covariance matrix for (a) active sonar, (b) passive sonar, and (c) fused sonar.

sonar as σ_θ increases.

5.6 Discussion and Conclusion

In this section, we investigate which sensing mechanism performs better overall in solving the SLAM problem based on the calculated metrics reported in the results section. Based on the defined metrics, an estimation algorithm performs well if it has low robot localization RMSE, low landmark localization RMSE, high number of detected landmarks, low maximum eigenvalue of the estimation covariance matrix, and low value in the chi-squared performance test. Here, we divide the simulation parameters into four different regions: high σ_θ and high α, high σ_θ and low α, low σ_θ and high α, and low σ_θ and low α. Then, we compare the performance of each sensing mechanism for each parameter region.

High $\boldsymbol{\sigma_\theta}$ and high $\boldsymbol{\alpha}$: When $\sigma_\theta > 0.3$ radians (about 17°) and $\alpha > \pi$, figures 5.3 and 5.6 show that the RMSE in robot and landmark localization increase in active and fused sensing and therefore, one might consider passive sonar a better sensing strategy. However, according

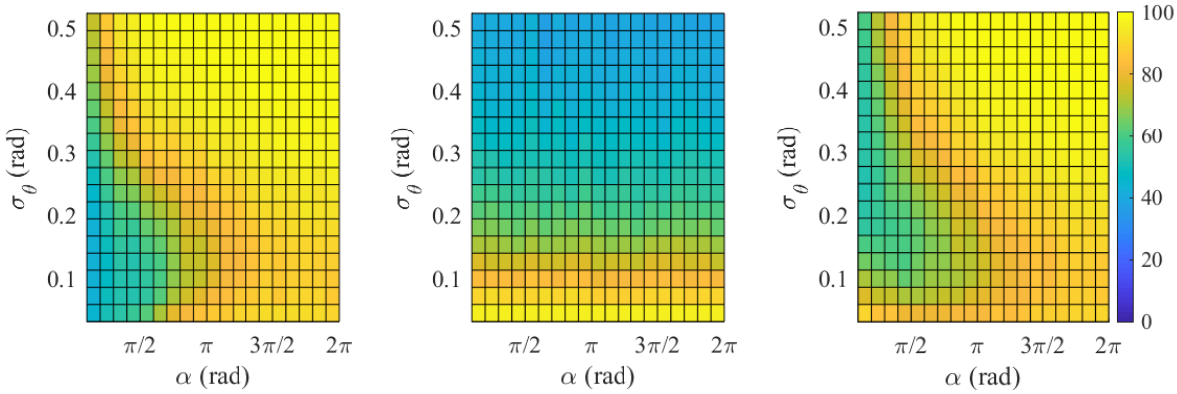

(a) Active sonar (b) Passive sonar (c) Fused sonar

Figure 5.8: Chi-squared filter performance test for (a) active sonar, (b) passive sonar, and (c) fused sonar.

to figure 5.7, the estimation algorithm based on passive sonar is not confident about its estimation. Recall that, due to the lack of range measurement in passive sonar, a landmark is localized after being detected in 5 different measurements by fusing the information of the first and 5th measurement. This will reduce the sensitivity of landmark initialization to bearing angle measurement noise in comparison to active sonar initialization which relies on only one bearing angle measurement. Therefore, an offset in bearing angle measurement can create large error in localizing a landmark (especially for those located farther away from the robot) and the EKF may not be able to correct it due to a small Kalman gain caused by lack of confidence in the measurement. Figure 5.5 shows that all the sensing strategies perform similarly in detecting landmarks around them. Finally, according to figure 5.8, both active and fused sonar perform poorly according to the chi-squared test but passive sonar shows better response. However, the lower chi-squared test value in passive sonar is merely due to large covariances in state estimation that leads to a small value of NEES (equation (5.8)). Therefore, a low chi-squared test by itself does not indicate a better performance of the EKF estimator using only passive sonar. In summary, for this region of parameters, none of the sensing mechanisms lead to an estimator with acceptable performance.

High $\boldsymbol{\sigma_\theta}$ and low $\boldsymbol{\alpha}$: When $\sigma_\theta > 0.3$ and $\alpha < \pi$, the passive sensing robot performance is similar to the previous case, that is RMSE in robot (figure 5.3) and landmark localization (figure 5.6) are small, yet the robot's state estimation is not confident as is evident by large maximum eigenvalue of the covariance of state estimation error (figure 5.7). Comparison of the RMSE in robot and landmarks localization for active and fused sonar simulations shows that the fused sonar has smaller error, yet it shows less confidence in the state vector estimation that manifests in large maximum eigenvalue of estimation error covariance. However, figure 5.5 shows that the fused sonar is better in detecting landmarks than active sensing. The chi-squared test result also shows that the fused sonar performs slightly better than the active sonar, however, this is also due to its large estimation covariance. Thus, when the opening angle is small, the fused sensing inherits the properties of both active and passive sonar.

Low $\boldsymbol{\sigma_\theta}$ and high $\boldsymbol{\alpha}$: When $\sigma_\theta < 0.3$ and $\alpha > \pi$, among different sensing strategies, passive sonar has the highest value of RMSE in robot and landmark locations while active sonar and fused sonar show the same performance according to figures 5.3 and 5.6. Figure 5 shows that all sensing mechanisms perform the same in finding landmarks around them. According to figure 5.7, all the sensing mechanisms show a good confidence in their estimation, yet the passive sonar loses confidence sooner as σ_θ increases. Finally, again due to implementation of EKF, none of the sensing approaches show a good performance according to the chi-squared consistency test. Therefore, as a summary we can say that both active and fused sensing strategies perform similarly as expected, since with large opening angle, fused sonar is mostly relying on active sonar information.

Low $\boldsymbol{\sigma_\theta}$ and low $\boldsymbol{\alpha}$: This is the region of parameter space that implementing fused sensing is beneficial. Comparing figures 5.3 and 5.6 shows that fused sonar has the smallest RMSE in robot and landmark localization comparing to active and passive sonar. Also, figure 5.7

shows that the estimation algorithm using fused sonar has more confidence in its estimation. The chi-squared consistency test shown in figure 5.8 suggests similarity between active sonar and fused sonar. Again, we should notice here that although active sonar seems to have a better consistency than fused and passive sonar, we believe that the fused sonar outperforms the other strategies in this region. This is due to the higher confidence of estimation when fused sonar is used compared to the active and passive sonar, especially when σ_θ is between 0.1 and 0.2 rad. Finally, figure 5.5 shows that fused sonar can detect more landmarks than active sonar. Therefore, in this parameter region, the fused sonar can detect more landmarks than active sonar, it can localize the landmarks that both algorithms detect more accurately, and it can localize the robot with more accuracy as well. In addition to lower error, the fused sonar case shows more confidence in its estimation and a slightly better consistency.

To summarize, the simulation results show that the EKF algorithm can perform better in solving SLAM problem using a fused sonar sensing strategy when the opening angle is less than π and the standard deviation of the bearing angle measurement noise, σ_θ, is less than 0.3 rad (about 17°). It is worth noting that this relatively small opening angle is consistent with beamwidths for currently-used commercial sonar sensors (see [100]). We intentionally used a wide range for σ_θ to make sure we see a response that is dominated by noise as our upper limit for σ_θ. Therefore, the result of this study is promising in practical implication. Nevertheless, the implementation of this work in practice comes with challenges such as data association or signal jamming in case of an extension to multi-agent robotic system as mentioned in introduction of this paper. We believe that this work will address solutions for interesting challenges for engineers and scientists in different disciplines and it may initiate a research path that will potentially alter the way we currently use sonar sensors for navigation.

Chapter 6

Conclusion

6.1 Summary and Conclusion

This work is inspired from group flight and sensing in bats. It is evident that when bats fly together, they eavesdrop on their conspecifics' echolocation signal. In other words, they fuse information through passive sonar with the information they gather by their active sonar. In engineered systems, however, when an agent uses an active sensor such as sonar, it filters every sound except the reflection of its own sound at the receiver. Therefore, the aforementioned information fusion between active and passive sonar is not currently implemented in engineered systems. The objective of this work is to investigate whether such information fusion observed in bats can improve the performance of the engineered systems.

We studied this problem in two different frameworks, the abstract agent-based framework and a more practical robotics framework. We used the Vicsek model, which is a a well-known flocking multi-agent model for the first part. In this model, every agent assumes the average

heading direction of its neighbors, disturbed by a noise. Since this noise is directly added to the agent's calculated heading, it is a process noise. To consider the effect of different sensing strategies, we modified this model to consider for both the process and measurement noise as explained in chapter 2. We found out that due to averaging between the heading direction of agents, the effect of measurement noise has less significant impact on the group behavior comparing to the process noise. This result is important since the passive sonar has less accuracy due to lack of range measurement in comparison to active sonar which can be modeled by adding stronger measurement noise value. Therefore, having stronger measurement noise modeling the integration of passive sonar will not immediately lead to loss the flocking behavior.

In chapter 3, we proposed a three dimensional Vicsek type model in which each agent are capable of perceiving their environment using both active and passive sensing. All the neighboring agents located within an active sensing cone in front of a specific agents are sensed by that agent actively, while other neighbors are sensed using passive sensing. Since the accuracy of the two sensing mechanism are different, the agent will have different confidence or trust in the information provided by active and passive sensing. This different trust is modeled using different noise values. The ability of the group to align depends on the active and passive noise magnitude as well as the opening angle of the active sensing cone. We performed sensitivity analysis on these parameters using Monte Carlo simulation. The results indicated that while the flocking behavior of the model will not always improved as the passive sensing is implemented, it will be improved for a range of parameters specifically when the opening angle is less than 180° and the passive sensing noise is not dramatically stronger than active sensing noise.

Beside agent-based abstract modeling, we studied the effectiveness of fusing active and passive sensing information in the framework of localization and mapping problem. In chapter

4, we solved the sound source tracking problem using only bearing angle measurement, when the dynamics of the sound source is not known, yet there are information available about its motion. This problem is important since the passive sonar is a bearing-only sensor and it is not practical to assume a dynamic for the sound source in advanced. We showed that it is possible to track the sound source if we can build a dynamic model using the different sensory information and a priori knowledge to track the sound source by Kalman filtering.

Finally in chapter 5, we studied the problem of simultaneous localization and mapping where the robot uses both active and passive sonar to build a map of the location of fixed landmarks and localize itself within that map using extended Kalman filter. The performance of the algorithm depend on the opening angle of active sonar and the measurement noise covariance of the active and passive sonar. We performed a numerical sensitivity analysis and found out that at a fixed active sonar measurement noise covariance, for the opening angle less than 180° and small passive sonar measurement noise covariance, the robot's performance improves when it implements passive sonar compared to when it only relies on active sonar.

The results of this work show that for the right range of the opening angle of sonar emitter and noise covariances, using passive sonar on top of active sonar improves the system's performance, whether it is in the framework of the group behavior of an abstract multi-agent system or in individual level we studied in the SLAM problem. Therefore, it is justified to further explore this idea in future research.

6.2 Future Direction

There are many ways to extend the work of this dissertation to obtain more insight about the underlying dynamics of multi-agent systems exploiting passive sensing as well as advancing to more practical engineered systems.

In the context of multi-agent Vicsek type model we investigated here, as it is mentioned in chapter 3, it seems that implementing passive sensing can affect the nature of phase transition. We performed numerical simulations of the system with up to the cube size of $L = 16$ for 100 Monte Carlo repetition. However, the results of this simulation cannot determine the nature of phase transition due to either finite size scaling effect or lack of statistical significance due to small number of Monte Carlo simulations. Further investigation is needed to answer this whether implementing passive sensing will change the nature of phase transition and if it does, how can such change in nature be explained by the underlying dynamics of the system.

This work can be further extended in solving the SLAM problem. One extension to this work is to solve the SLAM problem when the correspondence of the received echo is unknown. In this work, we assumed the correspondence of the signal is known since there are evidence that bats are able to distinguish the objects by analysing the echo received from them. However, object classification using sonar is still an active area of research. It is also possible to employ algorithms such as Joint Probabilistic Data Association (JPDA) used in multi-target tracking application to solve the data association problem when the signal correspondence is unknown. However, solving the data association problem, specifically when bearing-only sensors such as passive sonar is implemented is an open ended problem.

Using two robots eavesdropping on each other is another extension to the SLAM problem. The most important challenge here is to localize the other robot since its location follows an unknown dynamics in contrast with the fixed landmarks in the environment. It is important to note here that this problem is not exactly a multi-robot solution for SLAM problem since no communication and map sharing occurs between the robots. Nevertheless, it is possible to use eavesdropping in multi-robot SLAM scenario as well.

Experimental verification of this problem requires dealing with challenges such as specular

reflection of sound, sound source localization to extract bearing angle, and data association, as explained in more details in chapter 5. Also, it is required to identify the statistics of the process noise of the robot and the measurement noise of the sensors. In case of multi-robot application, one needs to think of a way to distinguish between the primary sound received directly from the other robot and its echo from the landmarks. Each robot can use a sound signal with unique signature to avoid signal jamming.

In further extension of this work to a swarm of robots, how to avoid signal jamming becomes an interesting and challenging problem. It is possible to define different signatures for each robot and use matched filter at the receiver to distinguish between the signals of different robots. Nevertheless, the number of patterns each robot can learn is restricted by memory limitation. In general, the strategies of avoiding signal jamming in a group of robots using active sensing is an open ended problem.

Bibliography

[1] Jens Krause and Graeme D. Ruxton. *Living in groups*. Oxford University Press, 2002.

[2] Nickolay I. Hristov, Louise C. Allen, and Brad A. Chadwell. *New Advances in the Study of Group Behavior in Bats*, chapter 14, pages 271–291. Springer New York, New York, NY, 2013.

[3] Henrik I. Christensen and Gregory D. Hager. *Sensing and estimation*, chapter 5, pages 91–112. Springer, New York, NY, 2016.

[4] A. Surlykke, P. E. Nachtigall, R. R. Fay, and A. N. Popper, editors. *Biosonar*. Springer, 2014.

[5] Chen Chiu, Wei Xian, and Cynthia F Moss. Flying in silence: echolocating bats cease vocalizing to avoid sonar jamming. *Proceedings of the National Academy of Sciences*, 105(35):13116–13121, 2008.

[6] Chad M. Topaz, Andrea L. Bertozzi, and Mark A. Lewis. A nonlocal continuum model for biological aggregation. *Bulletin of Mathematical Biology*, 68(7):1601, 2006.

[7] Tamás Vicsek, András Czirók, Eshel Ben-Jacob, Inon Cohen, and Ofer Shochet. Novel type of phase transition in a system of self-driven particles. *Phys. Rev. Lett.*, 75:1226–1229, Aug 1995.

[8] XS Zhou and Stergios I Roumeliotis. Multi robot slam map alignment with rendezvous. *Department of Computer Science & Engineering, University of Minnesota. Minnesota, USA*, 2005.

[9] Brian L. Partridge. The structure and function of fish schools. *Scientific American*, 246(6):114–123, 1982.

[10] Iztok Lebar Bajec and Frank H. Heppner. Organized flight in birds. *Animal Behaviour*, 78(4):777 – 789, 2009.

[11] Thomas Surrey, François Nédélec, Stanislas Leibler, and Eric Karsenti. Physical properties determining self-organization of motors and microtubules. *Science*, 292(5519):1167–1171, 2001.

[12] David A. Kessler and Herbert Levine. Pattern formation in dictyostelium via the dynamics of cooperative biological entities. *Physical Review E*, 48:4801–4804, Dec 1993.

[13] Christopher Dombrowski, Luis Cisneros, Sunita Chatkaew, Raymond E. Goldstein, and John O. Kessler. Self-concentration and large-scale coherence in bacterial dynamics. *Physical Review Letters*, 93:098103, Aug 2004.

[14] I. D. Couzin and N. R. Franks. Self-organized lane formation and optimized traffic flow in army ants. *Proceedings of the Royal Society of London B: Biological Sciences*, 270(1511):139–146, 2003.

[15] Cedric Sueur and Odile Petit. Organization of group members at departure is driven by social structure in macaca. *International Journal of Primatology*, 29(4):1085–1098, 2008.

[16] Eric Bonabeau. Agent-based modeling: methods and techniques for simulating human systems. *Proceeding of the National Academy of Sciences of the United States*, 99:7280–7287, 2002.

[17] Vijay Narayan, Sriram Ramaswamy, and Narayanan Menon. Long-lived giant number fluctuations in a swarming granular nematic. *Science*, 317(5834):105–108, 2007.

[18] Daniel L. Blair, T. Neicu, and A. Kudrolli. Vortices in vibrated granular rods. *Phys. Rev. E*, 67:031303, Mar 2003.

[19] Tamás Vicsek and Anna Zafeiris. Collective motion. *Physics Reports*, 517(3–4):71 – 140, 2012.

[20] Craig W. Reynolds. Flocks, herds and schools: a distributed behavioral model. *SIGGRAPH Comput. Graph.*, 21(4):25–34, August 1987.

[21] Iain D. Couzin, Jens Krause, Richard James, Graeme D. Ruxton, and Nigel R. Franks. Collective memory and spatial sorting in animal groups. *Journal of Theoretical Biology*, 218(1):1 – 11, 2002.

[22] H. Chaté, F. Ginelli, G. Grégoire, F. Peruani, and F. Raynaud. Modeling collective motion: variations on the Vicsek model. *The European Physical Journal B*, 64(3):451–456, 2008.

[23] András Czirók, Mária Vicsek, and Tamás Vicsek. Collective motion of organisms in three dimensions. *Physica A: Statistical Mechanics and its Applications*, 264(1–2):299 – 304, 1999.

[24] Jiaping Ren, Xinjie Wang, Xiaogang Jin, and Dinesh Manocha. Simulating flying insects using dynamics and data-driven noise modeling to generate diverse collective behaviors. *PLOS ONE*, 11(5):1–31, 05 2016.

[25] Jaime A. Pimentel, Maximino Aldana, Cristián Huepe, and Hernán Larralde. Intrinsic and extrinsic noise effects on phase transitions of network models with applications to swarming systems. *Phys. Rev. E*, 77:061138, Jun 2008.

[26] M. Aldana, V. Dossetti, C. Huepe, V. M. Kenkre, and H. Larralde. Phase transitions in systems of self-propelled agents and related network models. *Phys. Rev. Lett.*, 98:095702, Mar 2007.

[27] Wen-Qiang Tian, Dan Gao, Ju-Feng Luo, Wei-Yi Zhang, and Ying-Guan Wang. Effect of different types of noises on the formations of swarming systems: the sensing-noise and the acting-noise. *Modern Physics Letters B*, 28(23):1450186, 2014.

[28] Tian Wen-Qiang, Gao Dan, and Wang Ying-Guan. Self-organized collective crystal-like formations of the attractive/repulsive swarming system. *Modern Physics Letters B*, 28(01):1450003, 2014.

[29] Allison Kolpas, Jeff Moehlis, and Ioannis G. Kevrekidis. Coarse-grained analysis of stochasticity-induced switching between collective motion states. *Proceedings of the National Academy of Sciences*, 104(14):5931–5935, 2007.

[30] Igor S Aranson. Active colloids. *Physics-Uspekhi*, 56(1):79, 2013.

[31] Lucas Barberis and Fernando Peruani. Large-scale patterns in a minimal cognitive flocking model: Incidental leaders, nematic patterns, and aggregates. *Physical Review Letters*, 117:248001, Dec 2016.

[32] P. The Nguyen, Sang-Hee Lee, and V. Thanh Ngo. Effect of vision angle on the phase transition in flocking behavior of animal groups. *Physical Review E*, 92:032716, Sep 2015.

[33] Mihir Durve and Ahmed Sayeed. First-order phase transition in a model of self-propelled particles with variable angular range of interaction. *Physical Review E*, 93:052115, May 2016.

[34] Bao-Mei Tian, Han-Xin Yang, Wei Li, Wen-Xu Wang, Bing-Hong Wang, and Tao Zhou. Optimal view angle in collective dynamics of self-propelled agents. *Physical Review E*, 79(5):052102, 2009.

[35] Yu-Jian Li, Su Wang, Zhong-Lin Han, Bao-Mei Tian, Zhen-Dong Xi, and Bing-Hong Wang. Optimal view angle in the three-dimensional self-propelled particle model. *EPL (Europhysics Letters)*, 93(6):68003, 2011.

[36] Xiangyin Zhang, Songmin Jia, and Xiuzhi Li. Improving the synchronization speed of self-propelled particles with restricted vision via randomly changing the line of sight. *Nonlinear Dynamics*, 90(1):43–51, 2017.

[37] J-L Deneubourg, Serge Aron, Simon Goss, and Jacques Marie Pasteels. The self-organizing exploratory pattern of the argentine ant. *Journal of Insect Behavior*, 3(2):159–168, 1990.

[38] G. W. Max Westby. Electroreception and communication in electric fish. *Science Progress*, 69(274):291–313, 1984.

[39] Mary E Bates, Sarah A Stamper, and James A Simmons. Jamming avoidance response of big brown bats in target detection. *Journal of Experimental Biology*, 211(1):106–113, 2008.

[40] Martin K Obrist. Flexible bat echolocation: the influence of individual, habitat and conspecifics on sonar signal design. *Behavioral Ecology and Sociobiology*, 36(3):207–219, 1995.

[41] Chen Chiu, Puduru Viswanadha Reddy, Wei Xian, Perinkulam S Krishnaprasad, and Cynthia F Moss. Effects of competitive prey capture on flight behavior and sonar beam pattern in paired big brown bats, *Eptesicus fuscus*. *Journal of Experimental Biology*, 213(19):3348–3356, 2010.

[42] Wei Yang and Igor Zurbenko. Nonstationarity. *Wiley Interdisciplinary Reviews: Computational Statistics*, 2(1):107–115, 2010.

[43] Vladimir Privman. *Finite Size Scaling and Numerical Simulation of Statistical Systems*. World Scientific, 1990.

[44] Lord Rayleigh. On our perception of the direction of a source of sound. *Proceedings of the Musical Association*, 2:75–84, 1875.

[45] Andrew J Kolarik, Brian CJ Moore, Pavel Zahorik, Silvia Cirstea, and Shahina Pardhan. Auditory distance perception in humans: A review of cues, development, neuronal bases, and effects of sensory loss. *Attention, Perception, & Psychophysics*, 78(2):373–395, 2016.

[46] G. C. Stecker and F. J. Gallun. *Binaural Hearing, Sound Localization, and Spatial Hearing*, chapter Translational Perspectives in Auditory Neuroscience: Normal Aspects of Hearing, pages 383–433. Plural Publishing Inc., 2012.

[47] S. Argentieri, P. Danès, and P. Souères. A survey on sound source localization in robotics: From binaural to array processing methods. *Computer Speech and Language*, 34:87–112, 2015.

[48] Caleb Rascon and Ivan Meza. Localization of sound sources in robotics: A review. *Robotics and Autonomous Systems*, 96:184–210, 2017.

[49] Jingdong Chen, Jacob Benesty, and Yiteng Arden Huang. Time delay estimation in room acoustic environments: An overview. *EURASIP Journal on Advances in Signal Processing*, 2006(1):026503, 2006.

[50] Ajay Mahajan and Maurice Walworth. 3D position sensing using the differences in the time-of-flights from a wave source to various receivers. *IEEE Transactions on Robotics and Automation*, 17(1):91–94, 2001.

[51] Yeonjoo Shim, Jisung Park, and Jinwhan Kim. Relative navigation with passive underwater acoustic sensing. In *12th International Conference on Ubiquitous Robots and Ambient Intelligence (URAI)*, pages 214–217. IEEE, 2015.

[52] L. Kneip and C. Baumann. Binaural model for artificial spatial sound localization based on interaural time delays and movements of the interaural axis. *Journal of the Acoustical Society of America*, 124(5):3108–3119, 2008.

[53] B. G. Shinn-Cunningham, S. Santarelli, and N. Kopco. Tori of confusion: Binaural localization cues for sources within reach of a listener. *Journal of Acoustical Society of America*, 107:1627–1636, 2000.

[54] S. J. Cho, A. Ovcharenko, and U. p. Chong. Front-back confusion resolution in 3d sound localization with HRTF databases. In *The 1st International Forum on Strategic Technology*, pages 239–243, 2006.

[55] Duncan Tamsett. Binaural range finding from synthetic aperture computation as the head is turned. *Robotics*, 6(2):10, 2017.

[56] Yan-Chen Lu and Martin Cooke. Binaural estimation of sound source distance via the direct-to-reverberant energy ratio for static and moving sources. *IEEE Transactions on Audio, Speech, and Language Processing*, 18(7):1793–1805, 2010.

[57] K. Takami, T. Furukawa, M. Kumon, and L. C. Mak. Non-field-of-view indoor sound source localization based on reflection and diffraction. In *IEEE International Conference on Multisensor Fusion and Integration for Intelligent Systems*, pages 59–64, Sept 2015.

[58] Zhiwei Liang, Xudong Ma, and Xianzhong Dai. Robust tracking of moving sound source using multiple model kalman filter. *Applied Acoustics*, 69(12):1350–1355, 2008.

[59] Y. Lu and M. Cooke. Motion strategies for binaural localisation of speech sources in azimuth and distance by artificial listeners. *Speech Communication*, 53(5):622 – 642, 2011.

[60] Quan V Nguyen, Francis Colas, Emmanuel Vincent, and François Charpillet. Localizing an intermittent and moving sound source using a mobile robot. In *2016 IEEE/RSJ International Conference on Intelligent Robots and Systems (IROS)*, pages 1986–1991. IEEE, 2016.

[61] Yaakov Bar-Shalom, X Rong Li, and Thiagalingam Kirubarajan. *Estimation with applications to tracking and navigation: Theory algorithms and software*. John Wiley & Sons, 2004.

[62] Enrique Garcia, José A Paredes, Fernando J Álvarez, M Carmen Pérez, and Juan Jesús García. Spreading sequences in active sensing: A review. *Signal Processing*, 106:88–105, 2015.

[63] John J Leonard and Hugh F Durrant-Whyte. *Directed sonar sensing for mobile robot navigation*, volume 175. Springer Science & Business Media, 2012.

[64] Suhwan Kim, Bonhwa Ku, Wooyoung Hong, and Hanseok Ko. Performance comparison

of target localization for active sonar systems. *IEEE transactions on aerospace and electronic systems*, 44(4):1371–1380, 2008.

[65] Antoni Burguera, Yolanda González, and Gabriel Oliver. Sonar sensor models and their application to mobile robot localization. *Sensors*, 9(12):10217–10243, 2009.

[66] M Brown. Feature extraction techniques for recognizing solid objects with an ultrasonic range sensor. *IEEE Journal on Robotics and Automation*, 1(4):191–205, 1985.

[67] KS Nagla, Moin Uddin, and Dilbag Singh. Improved occupancy grid mapping in specular environment. *Robotics and Autonomous Systems*, 60(10):1245–1252, 2012.

[68] Lindsay Kleeman and Roman Kuc. *Sonar Sensing*, pages 753–782. Springer International Publishing, Cham, 2016.

[69] Billur Barshan and Roman Kuc. Differentiating sonar reflections from corners and planes by employing an intelligent sensor. *IEEE Transactions on Pattern Analysis and Machine Intelligence*, 12(6):560–569, 1990.

[70] Peter Krammer and Herbert Schweinzer. Localization of object edges in arbitrary spatial positions based on ultrasonic data. *IEEE Sensors Journal*, 6(1):203–210, 2006.

[71] S Walter. The sonar ring: Obstacle detection for a mobile robot. In *Proceedings. 1987 IEEE International Conference on Robotics and Automation*, volume 4, pages 1574–1579. IEEE, 1987.

[72] Saeid Fazli and Lindsay Kleeman. A real time advanced sonar ring with simultaneous firing. In *2004 IEEE/RSJ International Conference on Intelligent Robots and Systems (IROS)(IEEE Cat. No. 04CH37566)*, volume 2, pages 1872–1877. IEEE, 2004.

[73] Juan D Tardós, José Neira, Paul M Newman, and John J Leonard. Robust mapping and localization in indoor environments using sonar data. *The International Journal of Robotics Research*, 21(4):311–330, 2002.

[74] David Ribas, Pere Ridao, and José Neira. *Underwater SLAM for structured environments using an imaging sonar*, volume 65. Springer, 2010.

[75] TJ Chong, XJ Tang, CH Leng, M Yogeswaran, OE Ng, and YZ Chong. Sensor technologies and simultaneous localization and mapping (slam). *Procedia Computer Science*, 76:174–179, 2015.

[76] Hemani Kaushal and Georges Kaddoum. Underwater optical wireless communication. *IEEE Access*, 4:1518–1547, 2016.

[77] Jeanette A Thomas, Cynthia F Moss, and Marianne Vater. *Echolocation in bats and dolphins*. University of Chicago Press, 2004.

[78] Yanqing Fu, Philip Caspers, and Rolf Müller. A dynamic ultrasonic emitter inspired by horseshoe bat noseleaves. *Bioinspiration & biomimetics*, 11(3):036007, 2016.

[79] Xiaoyan Yin and Rolf Müller. Fast-moving bat ears create informative doppler shifts. *Proceedings of the National Academy of Sciences*, 116(25):12270–12274, 2019.

[80] Luhui Yang, Allison Yu, and Rolf Müller. Design of a dynamic sonar emitter inspired by hipposiderid bats. *The Journal of the Acoustical Society of America*, 141(5):3485–3485, 2017.

[81] Roman Kuc. Generating cognitive maps using echo features from a biomimetic audible sonar. *The Journal of the Acoustical Society of America*, 145(4):2084–2093, 2019.

[82] Payman Rajai, Matthew Straeten, Shahpour Alirezaee, and Mohammed Jalal Ahamed. Binaural sonar system for simultaneous sensing of distance and direction of extended barriers. *IEEE Sensors Journal*, 19(24):12040–12049, 2019.

[83] Itamar Eliakim, Zahi Cohen, Gabor Kosa, and Yossi Yovel. A fully autonomous terrestrial bat-like acoustic robot. *PLoS computational biology*, 14(9):e1006406, 2018.

[84] Aaron J Corcoran and William E Conner. Bats jamming bats: Food competition through sonar interference. *Science*, 346(6210):745–747, 2014.

[85] Masoud Jahromi Shirazi and Nicole Abaid. Tracking a sound source with unknown dynamics using bearing-only measurements based on a priori information. In *2019 American Control Conference (ACC)*, pages 4491–4496. IEEE, 2019.

[86] Murat Aytekin, Elena Grassi, Manjit Sahota, and Cynthia F Moss. The bat head-related transfer function reveals binaural cues for sound localization in azimuth and elevation. *The Journal of the Acoustical Society of America*, 116(6):3594–3605, 2004.

[87] Ngai Ming Kwok, Gamini Dissanayake, and Quang Phuc Ha. Bearing-only slam using a sprt based gaussian sum filter. In *Proceedings of the 2005 IEEE International Conference on Robotics and Automation*, pages 1109–1114. IEEE, 2005.

[88] Thomas Lemaire, Simon Lacroix, and Joan Sola. A practical 3d bearing-only slam algorithm. In *2005 IEEE/RSJ International Conference on Intelligent Robots and Systems*, pages 2449–2454. IEEE, 2005.

[89] Adizul Ahmad, Shoudong Huang, and Gamini Dissanayake. Accurate large-scale bearing-only slam by map joining. In *2010 Australasian Conference on Robotics and Automation*, 2010.

[90] Matthew C Deans and Martial Hebert. *Bearings-only localization and mapping*. PhD thesis, Citeseer, 2005.

[91] Ralph Simon, Stefan Rupitsch, Markus Baumann, Huan Wu, Herbert Peremans, and Jan Steckel. Bioinspired sonar reflectors as guiding beacons for autonomous navigation. *Proceedings of the National Academy of Sciences*, 2020.

[92] Sebastian Thrun, Wolfram Burgard, and Dieter Fox. *Probabilistic robotics*. MIT press, 2005.

[93] Thomas E Fortmann, Yaakov Bar-Shalom, and Molly Scheffe. Multi-target tracking using joint probabilistic data association. In *1980 19th IEEE Conference on Decision and Control including the Symposium on Adaptive Processes*, pages 807–812. IEEE, 1980.

[94] Albert Costa, George Kantor, and Howie Choset. Bearing-only landmark initialization with unknown data association. In *IEEE International Conference on Robotics and Automation, 2004. Proceedings. ICRA'04. 2004*, volume 2, pages 1764–1770. IEEE, 2004.

[95] Chao-Lei Wang, Tian-Miao Wang, Jian-Hong Liang, Yi-Cheng Zhang, and Yi Zhou. Bearing-only visual slam for small unmanned aerial vehicles in gps-denied environments. *International Journal of Automation and Computing*, 10(5):387–396, 2013.

[96] Mitch Bryson and Salah Sukkarieh. Building a robust implementation of bearing-only inertial slam for a uav. *Journal of Field Robotics*, 24(1-2):113–143, 2007.

[97] Rodrigo Munguía and Antoni Grau. Concurrent initialization for bearing-only slam. *Sensors*, 10(3):1511–1534, 2010.

[98] Randall C Smith and Peter Cheeseman. On the representation and estimation of spatial uncertainty. *The international journal of Robotics Research*, 5(4):56–68, 1986.

[99] Mark L Psiaki. The blind tricyclist problem and a comparative study of nonlinear filters: A challenging benchmark for evaluating nonlinear estimation methods. *IEEE Control Systems Magazine*, 33(3):40–54, 2013.

[100] Teledyne Marine. Acoustic transducers. http://www.teledynemarine.com/acoustic-transducers/, Accessed August 30, 2020.